Project: “Monitoring Sea-water intrusion in coastal aquifers and Testing pilot projects for its mitigation” Interreg CBC Italy-Croatia 2014.-2020.

Priority Axis: Safety and resilience

Specific objective: Improve the climate change monitoring and planning of adaptation measures tackling specific effects, in the cooperation area

(D_4.1.4) Decision upon recommendations and actions for salt water intrusion mitigation made: report on positive and negative effects of potential actions

Work Package 4: Testing

Activity 1: Neretva coastal plain

Partner in charge: PP4 (UNIST-FGAG)

Partners involved: PP4 (UNIST-FGAG), PP5 (CROATIAN WATERS), PP6 (DUNEA)

Final version

Public report

September, 2022

Content

Mitigation measures - overview

Sea water intrusion along the Mediterranean basin

The Mediterranean area is undergoing intensive demographic, social, cultural, economic, and environmental changes. This generates multiple environmental pressures such as increased demand for water resources, generation of pollution related to wastewater discharge, and land consumption. In the Mediterranean area, recent climate change studies forecast large impacts on the hydrologic cycle. Thus, in the next years, surface and ground-water resources will be gradually more stressed, especially in coastal areas.

About 450 million people live along the 46,000 km of the Mediterranean basin, belonging to as many as 20 different nationalities, and are concentrated above all in the fertile coastal plains, where the density of inhabitants can reach up to 1300 in/km^2. This strong demographic pressure, which is also expected to rapidly increase, especially along the coasts in the next decade, places evident stresses on both SW and GW resources. Moreover, in the Mediterranean, the GW resources are not distributed in a homogeneous fashion both at a regional scale and within each country. Thus, the increase in GW exploitation poses a severe risk for the availability of water resources, and the resulting scarcity is a major concern in most countries of the Mediterranean region.

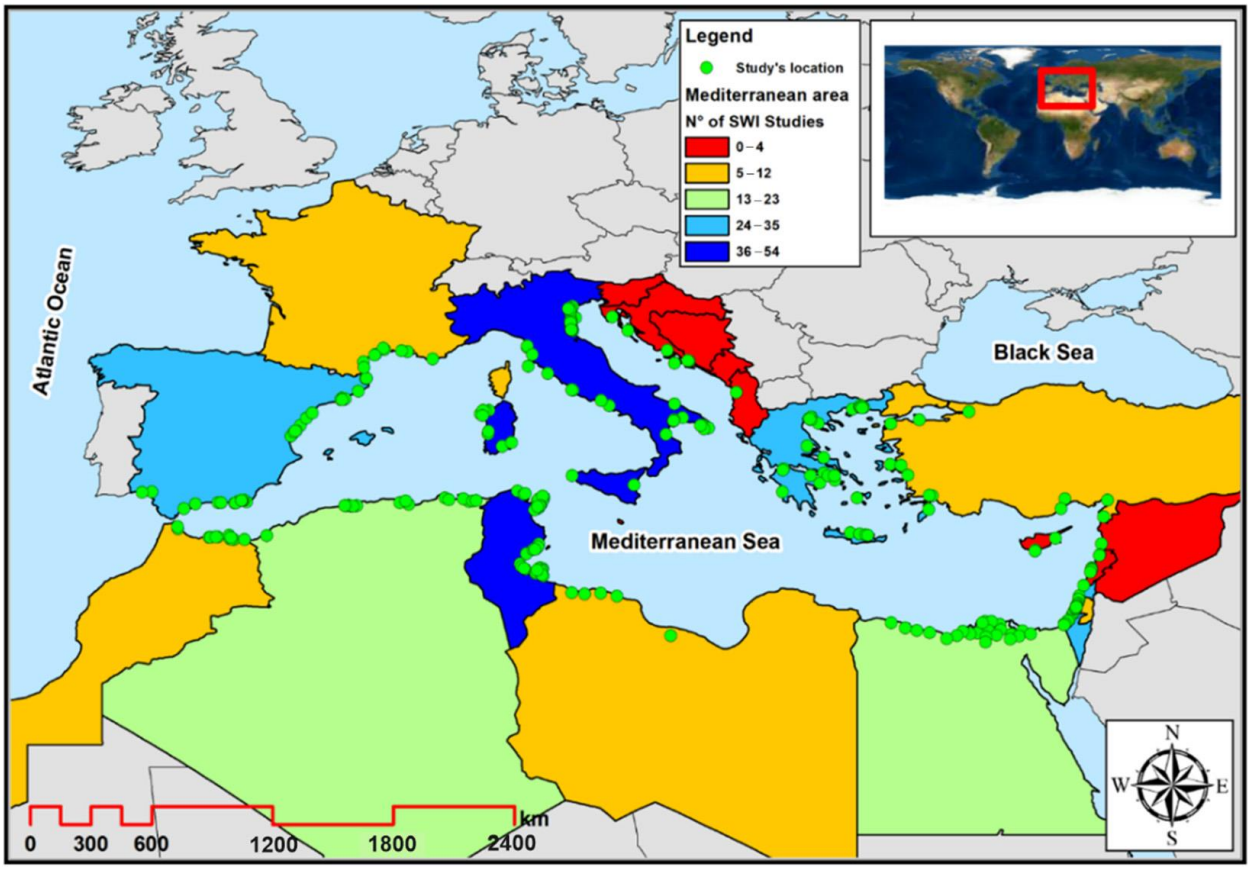

Figure 1 Distribution of the studies focusing on groundwater (GW) salinization along the Mediterranean

An interesting subdivision of the published studies can be deduced if the coastal extension of each country bordering the Mediterranean basin is taken into consideration. In this case it is evident that the contribution of the countries of the southern Mediterranean shore is much more intense, with Palestine showing the highest number of works published every 100 km of coastline. Since the graph is in logarithmic scale, the following countries can be grouped together starting from: (i) Palestine and Israel; (ii) Tunisia, Lebanon, Egypt, Morocco, Spain, Algeria, and France; (iii) Italy, Syria, Turkey,Cyprus; (iv) Libya Albania, Greece and Croatia have much less studies respect to their coastal extension. This emphasizes a greater interest in the problem of

GW salinization precisely in countries where the issues relating to water scarcity are yet more pressing. An exception is Greece, even if is highly affected by water scarcity, since its coastal extension is huge with respect to its area. While Libya and Syria have low values despite their extremely high water scarcity because military conflicts have played a role.

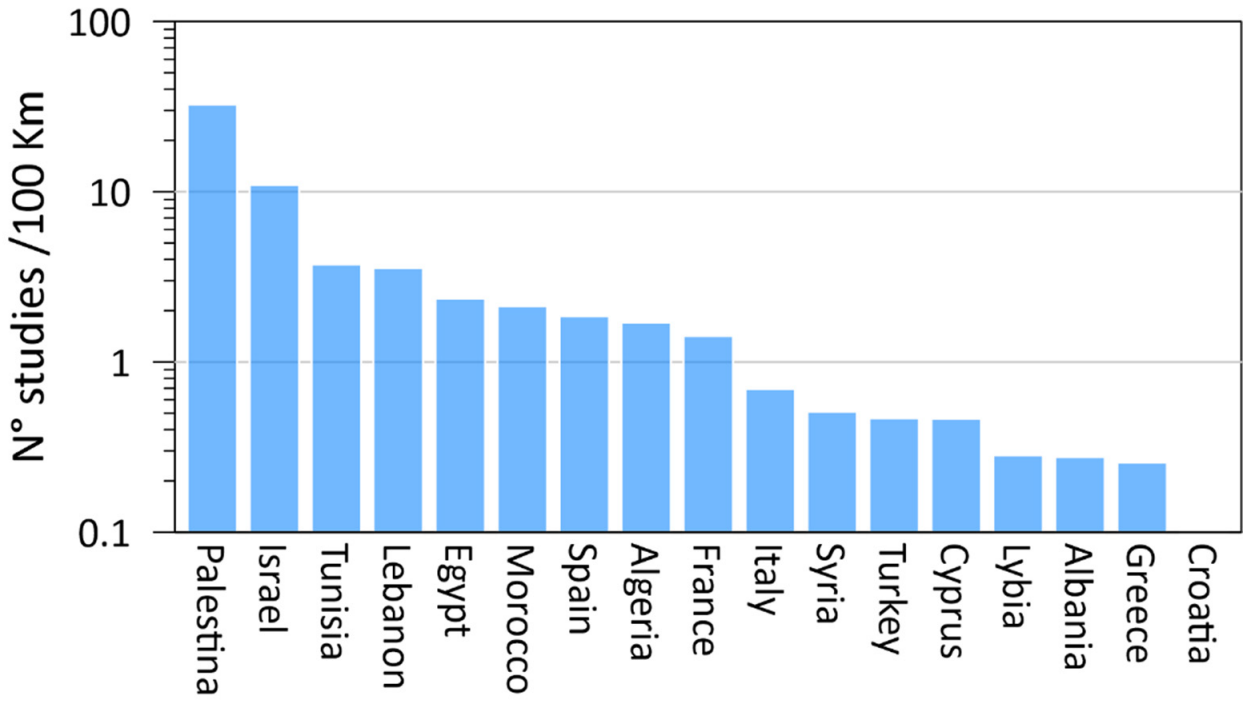

Figure 2 Number of studies focusing on GW salinization with respect to the coastal extension of each country along the Mediterranean

As regards the extension of the studies focusing on GW salinization in the Mediterranean, the vast majority have an extension between 102 and 103 km^2; a fair number of studies have been carried out on more limited areas, extended between 10 and 102 km2, while regional studies are far more scarce. Only very few studies on the entire Nile delta cover an area greater than 106 km^2, while some studies in Egypt, Israel, and Tunisia cover areas between 104 and 105 km^2. The scarcity of studies at the regional level does not only depend on the frequent need to solve

specific local problems that increase the number of pilot and small-scale studies, but also, and perhaps above all, on the lack of extensive and homogeneous monitoring networks that can allow a consistent characterization of a large portion of the coast.

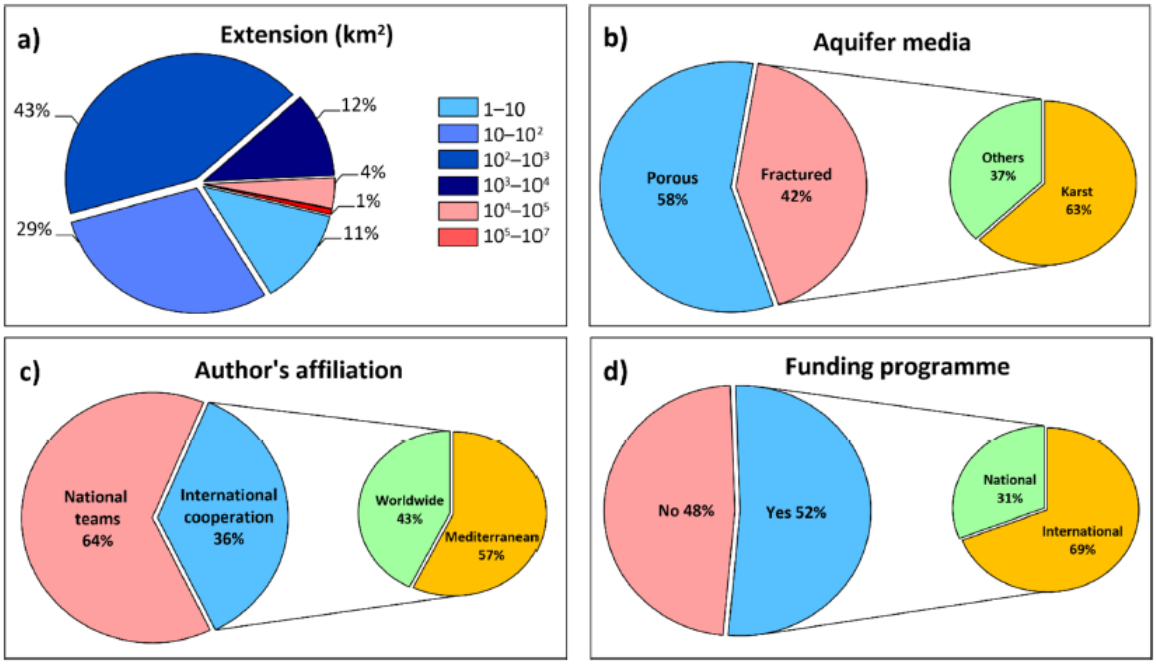

Figure 3 Geographical extension (a) and type of aquifer (b) of the studies focusing on GW salinization; relevance of international cooperation (c) and funding programmes (d) within the selected studies

In the porous aquifers, the largest number of studies concerns the main deltas of the Mediterranean (Nile, Po, Rhône, Ebro, and Llobregat), while in the fractured aquifers, most of the studies investigate karst aquifers, especially along the southeastern coast of the Mediterranean basin.

Subsurface barriers

Subsurface barriers have been used as one of the engineering measures to prevent saltwater intrusion in the coastal aquifers in China. However, the effectiveness of those barriers has not been studied thoroughly. The impact of the different permeability of the subsurface barriers to the migration distance and diffusion of saltwater front was also tested in the laboratory and simulated by using the two-dimensional numerical model.

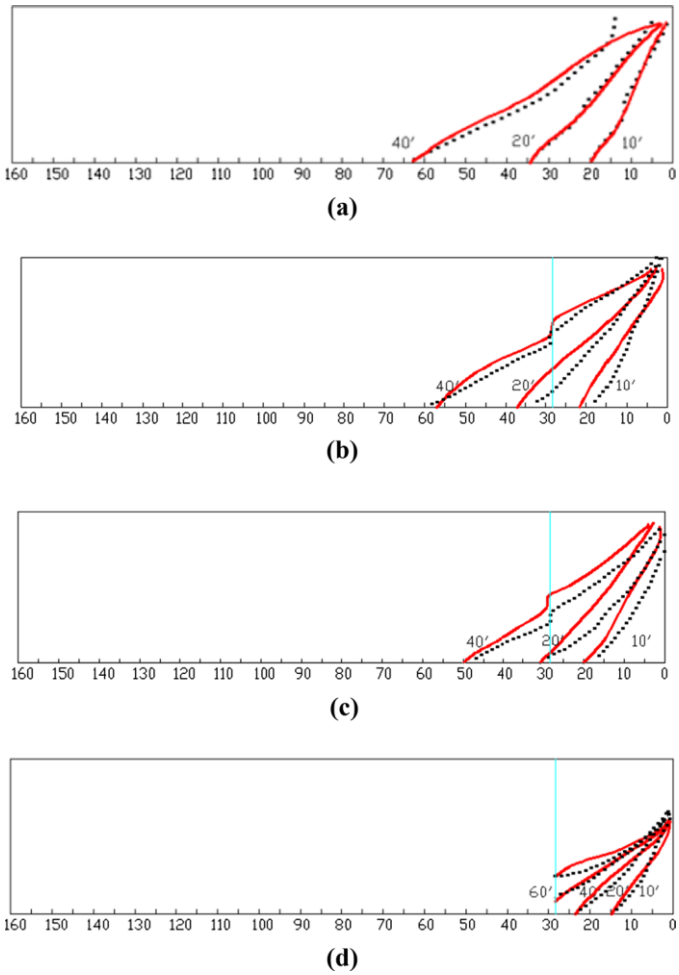

Figure 4 The fitting results of the saltwater intrusion simulation with and without subsurface barriers: a) without subsurface barrier, b) K = 9.9 × 10−7 m/s, c) K = 1.3 × 10−7 m/s, d) K = 3.7 × 10−8 m/s

The influence of the subsurface barriers with different permeability coefficients on the saltwater intrusion rate could be analyzed from the concentration variation of the observation point.

There was difference for the concentration variation of the observation point with and without subsurface barriers. The concentration of observation point increased rapidly and reached saturation in less than half an hour without subsurface barrier, which indicated that the salt water migrated to the observation point in less than half an hour. With the decrease in the permeability coefficient of subsurface barriers, the time to saturate the observation.

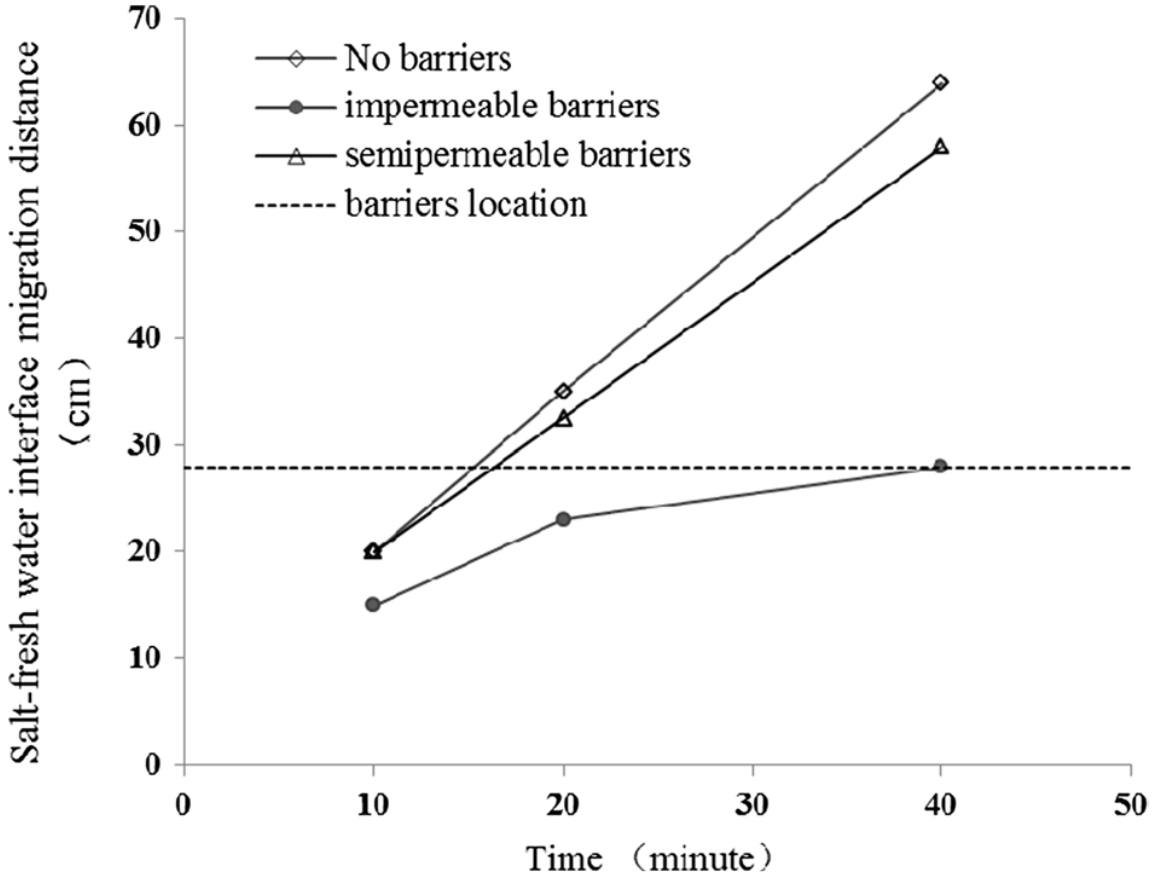

Figure 5 Salt–fresh water interface migration distance with time

Then, the salt–fresh water interface migration distance with time was different without subsurface barrier ($K = 2.2 \times 10^{-3}$ m/s) and with subsurface barriers that $K = 9.9 \times 10^{-7}$ and $K = 3.7 \times 10^{-8}$ m/s. We could see that the salt–fresh water interface migration distance with no barriers ($K = 2.2 \times 10^{-3}$ m/s) was longer than that with semipermeable barriers ($K = 9.9 \times 10^{-7}$ m/s), and the migration distance was the shortest with impermeable barriers ($K = 3.7 \times 10^{-8}$ m/s) when the migration time was the same. With time going, the difference in salt–fresh water interface migration distance between no barriers and semipermeable barriers and impermeable barriers became larger. When it was in 40 min, the salt–fresh water interface migration distance was no longer increasing, which indicated that the salt water cannot go through the barriers. The salt–fresh water interface migration distance increased linearly with time increasing when without subsurface barriers and with semipermeable barriers, while it increased in logarithmic with time increasing when with impermeable subsurface barriers.

From the discussions above, we could see that it had no effect on saltwater intrusion when the hydraulic conductivity was larger than 10^{-3} m/s, while it could well prevent the seawater intrusion when the hydraulic conductivity was less than 10^{-8} m/s. This means that low permeability of subsurface barriers has good effectiveness of mitigation of saltwater intrusion. It is the reason that the grouting cement is often used as subsurface barrier materials in the engineering practice in China.

Subsurface barriers and fresh water injection

Freshwater recharge wells and underground flow barriers are among several methods proposed for controlling saltwater intrusion (SWI) into coastal aquifers. For the barrier wall and freshwater injection experiments, the porous medium tank and both side reservoirs were initially filled with distilled water. Drainage pipes were used to adjust the constant head to 31.4 and 30.5 cm, measured from the bottom of the sand tank reservoir for the freshwater and the saltwater reservoirs respectively. The estimated fluctuations of the head during the experiments were ± 1.0 mm. The head difference between the freshwater and the saltwater was 0.90 cm with hydraulic gradient (0.01209) is consistent with previous laboratories studies using similar experimental set up (Goswami and Clement 2007; Chang and Clement 2012; Abdoulhalik et al. 2017) and within the range of hydraulic gradient measured at some field sites (Attanayake and Sholley 2007). The hydraulic gradient between the two heads produced a flow from the freshwater reservoir towards the saltwater reservoir. Darcy's law was used to estimate the hydraulic conductivity (K) of the porous medium in the sand tank, based on the hydraulic gradient and the measured freshwater flow from the drainage pipes. After measuring the flow, the shut-off wall is then inserted to separate the saltwater reservoir from the main middle tank. After that, the freshwater in the saltwater reservoir was removed and replaced by the red saltwater solution from the saltwater tank below.

Figure 6 Sand box model

The SEAWAT program (Guo and Langevin 2002) was used to simulate SWI for the barrier wall and freshwater injection experiments. The SEAWAT program combines both MODFLOW and MT3DMS. In the variable-density flow (VDF) process of the SEAWAT program, the well-established MODFLOW is used as a familiar tool for solving the equations for the variable-density groundwater flow system by means of the finite-difference method (FDM) (Guo and Langevin 2002).

Figure 7 shows the steady-state results for the SWI wedge after installing the flow barriers at depths of db = 13.5, 15.5, 17.5 and 20.5 cm. The average values of hydraulic conductivity and

porosity are found to be 0.60 cm/s and 0.43 respectively. The length of the SWI wedge in the steady-state condition is 48.00 cm, measured from the saltwater reservoir. After 70 min from the installation of the flow barrier to a depth of 13.5 cm, the SWI wedge had gradually retreated and the steady-state toe position had retreated to 38.0 cm, with a repulsion ratio of about 20.8%.

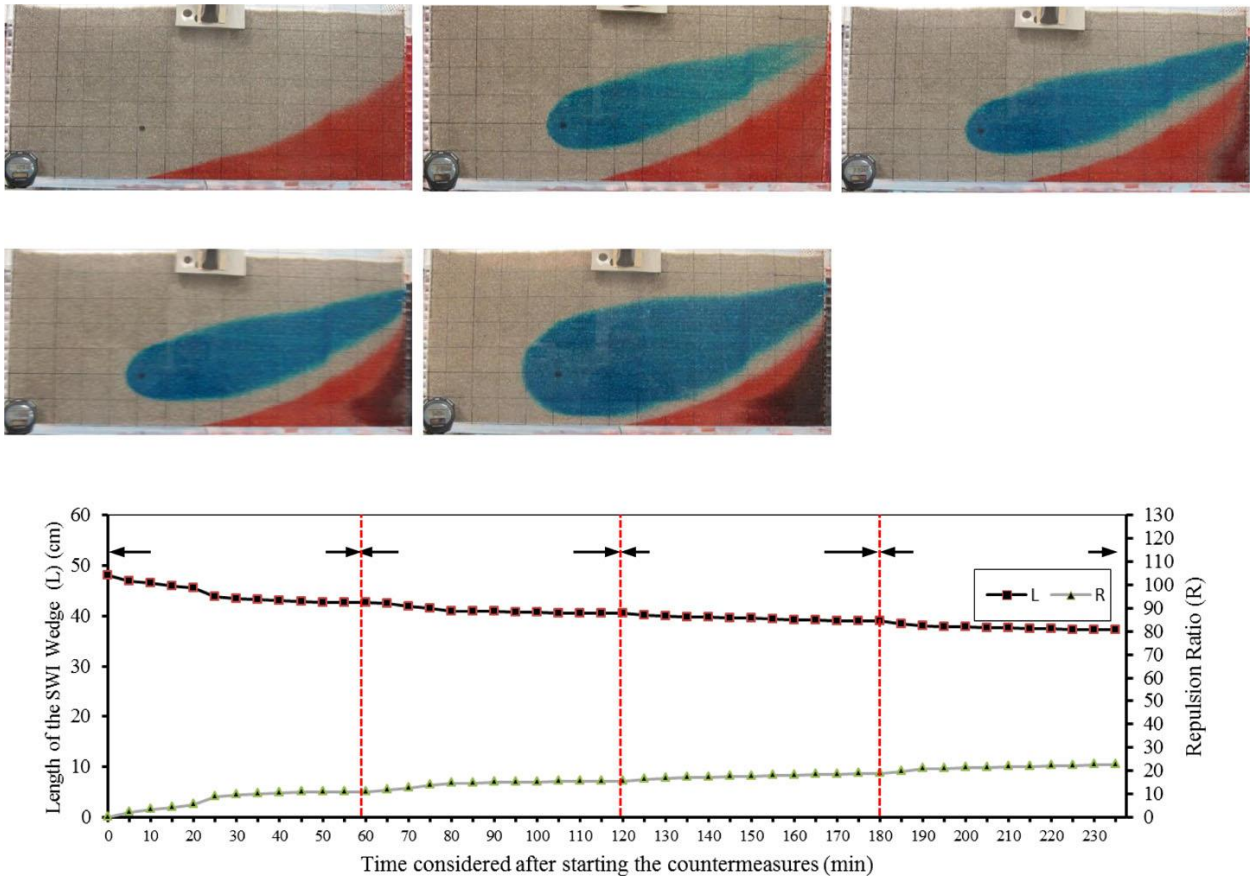

Figure 7 SWI experiments results with injection rate a Steady state, b Qi = 20 cm3/min, c Qi = 30 cm3/min, d Qi =40 cm3/min, e Qi = 50 cm3/min and f Length of the SWI wedge and repulsion ratio through the time

On the other hand, the scenarios of the freshwater injection experiments through an injection point confirmed that the most effective value of repulsion ratio of the SWI wedge was achieved with the highest value of injection flow rate. The most practicable freshwater injection rate

should be applied in order to achieve maximum R. Increasing the freshwater injection ratio (Qi/Q) through point injection from 0.22 to 0.56 led to the repulsion ratio increasing from 10.93 to 22.39%. Embedding the barrier wall into the aquifer after injecting the freshwater through the well, as a combined method of controlling the SWI in unconfined coastal aquifers achieved greater R for the SWI compared with a barrier wall or freshwater injection separately. Embedding the barrier wall further into the aquifer leads to a decrease in the opening below the barrier wall and an increase in the pressure head and the flow from the freshwater to the saltwater side, which forces the SWI to become attenuated towards the saltwater side.

Well abstraction

Laboratory experiments were completed in a 2D flow tank for a homogeneous aquifer where the time evolution of the saltwater wedge was analyzed during the upcoming and the receding phase. The SEAWAT code was used for validation purposes and to thereafter examine the sensitivity of the critical pumping rate and the critical time (the time needed for the saltwater to reach the well) to the well design and hydrogeological parameters. Results showed that the critical pumping rate and the critical time were more sensitive to the variations of the well location than the well depth. The critical time increased with increasing the location and depth ratios following a relatively linear equation. For all the configurations tested, the lowest critical pumping rate was found for the lower hydraulic conductivity, which reflects the vulnerability of low permeability aquifers to salinization of pumping wells.

The results show that numerical model predicted very well the seaward motion of the saltwater wedge observed in the physical model. The model reproduced similar rapid seaward motion of the tip of the cone away from the well as well as the subsequent lowering of the freshwater-saltwater interface until it regained its natural relatively straight shape at steady state. The widening of the transition zone was also exhibited in the numerical model, although slightly narrower than the experimental model. The receding phase reached steady state relatively quicker in the numerical model at t = 15 min, while some changes could still be observed in the experimental wedge, albeit merely located within the transition zone.

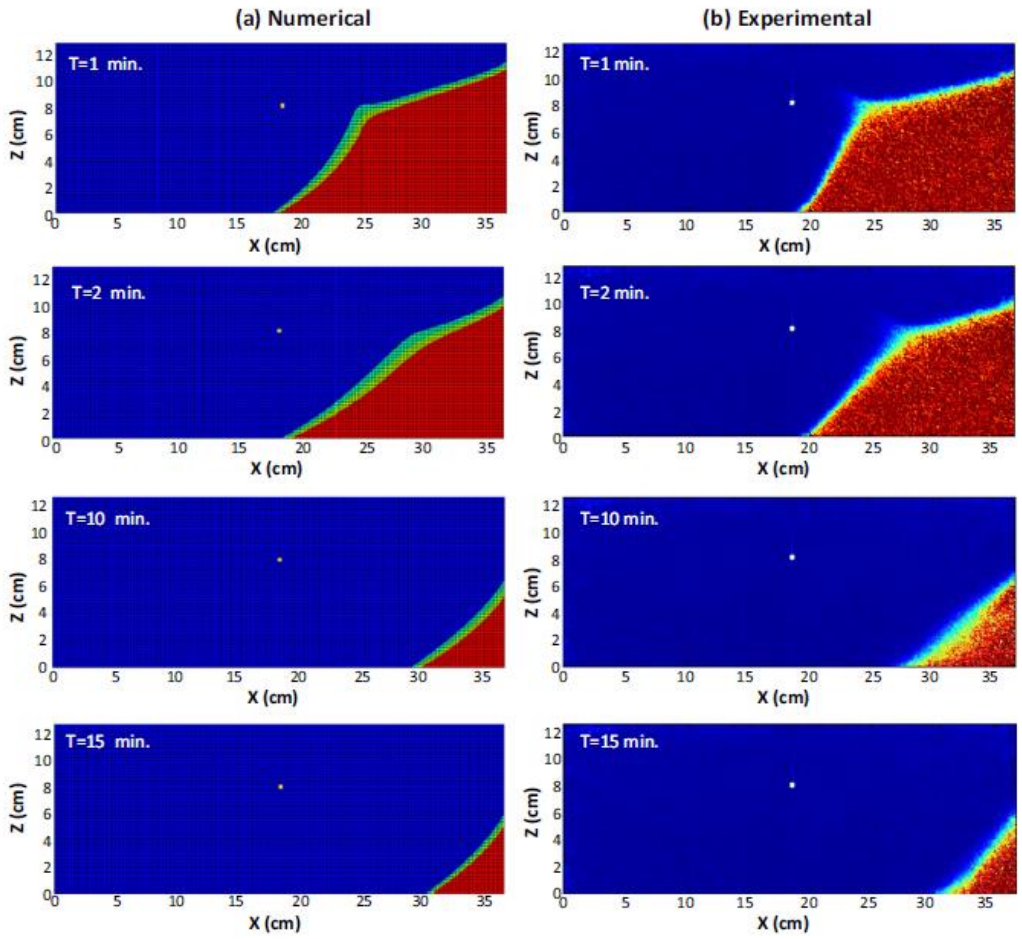

Figure 8 Comparison between experimental and numerical saltwater receding process at different time step from the start of turning off pumps a) Numerical images b) Experimental concentration color maps

Figure 8 shows the quantitative comparison between the transient experimental and numerical toe length results. The results show that the numerical toe length data agree well with the experimental results for both the upcoming and receding phases, despite the toe length was slightly overestimated in the numerical model. This mismatch might be due to possible minor source of heterogeneity commonly associated with the packing of the beads, while the numerical model assumes perfectly homogenous medium. Other factors such as tiny fluctuations in the

water levels caused by the surrounding vibrations may also contribute to this minor discrepancy. In general, the results show good agreement between numerical and experimental shape of the saltwater plume and the toe length data.

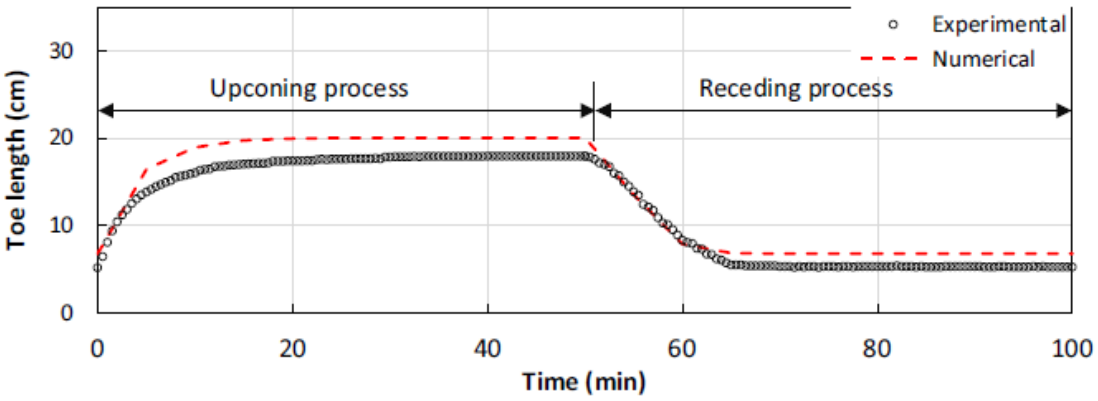

Figure 9 Comparison between transient experimental and numerical toe length data

The resulting model was used to perform additional simulations to explore the sensitivity of the critical pumping rate and the critical time to the design parameters of the well and the main hydrogeological parameters in an unconfined aquifer model. The results show that the critical pumping rate and the critical time were more sensitive to the variations in the well location than the well depth. The critical time increased with increasing the well location and depth ratios following relatively simple linear equation. For all configurations tested, the lowest critical pumping rate was found for the lowest hydraulic conductivity, which reflects the vulnerability of low permeability aquifers to salinization because of freshwater extractions. In addition, higher saltwater densities facilitated the saltwater upcoming mechanism. The influence of the saltwater density on the critical time was more significant for wells located farther away from the initial position of the interface. The results show that increasing the dispersivity only induced very little change on the critical pumping rate. For a fixed pumping rate, the critical time decreased with

increasing dispersivity, which suggests that higher dispersive systems would tend to induce faster upcoming mechanism.

Cut off wall

Artificial subsurface barriers are among several countermeasures proposed to control seawater intrusion into coastal aquifers. We performed experimental and numerical studies to investigate the dynamics of residual saltwater trapped in the storage area upon installation of cutoff walls.

We compared saltwater wedge toe positions from the 40-cm and 20-cm cutoff wall experiments. The residual saltwater wedge toe advanced farther after installation of the 40-cm cutoff wall than the 20-cm wall. The net advance of the residual saltwater is only 0.7-cm after about 20 min in the 20-cm wall experiment compared to the 5.1-cm advance after about 30 min in the 40-cm wall experiment. The higher wall produced a smaller opening for freshwater discharge and larger increased water levels, and required a longer flow path for the freshwater to travel. These circumstances resulted in more opportunity time for density difference to take effect before the new flow field was able to counterbalance and initiate residual saltwater removal. In relation to this, the removal of residual saltwater behind the shorter 20-cm cutoff was completed in 1 day, compared to 2 days behind the 40-cm cutoff wall. In each case, the rate of residual saltwater removal was constant, but slower for the 40-cm wall. Again this is due to the longer flow path the freshwater, carrying low concentration salt, had to flow before removal. The greater crest height and smaller size of the opening for the 40-cm wall increased the time for the freshwater discharge to flush the dispersed residual saltwater.

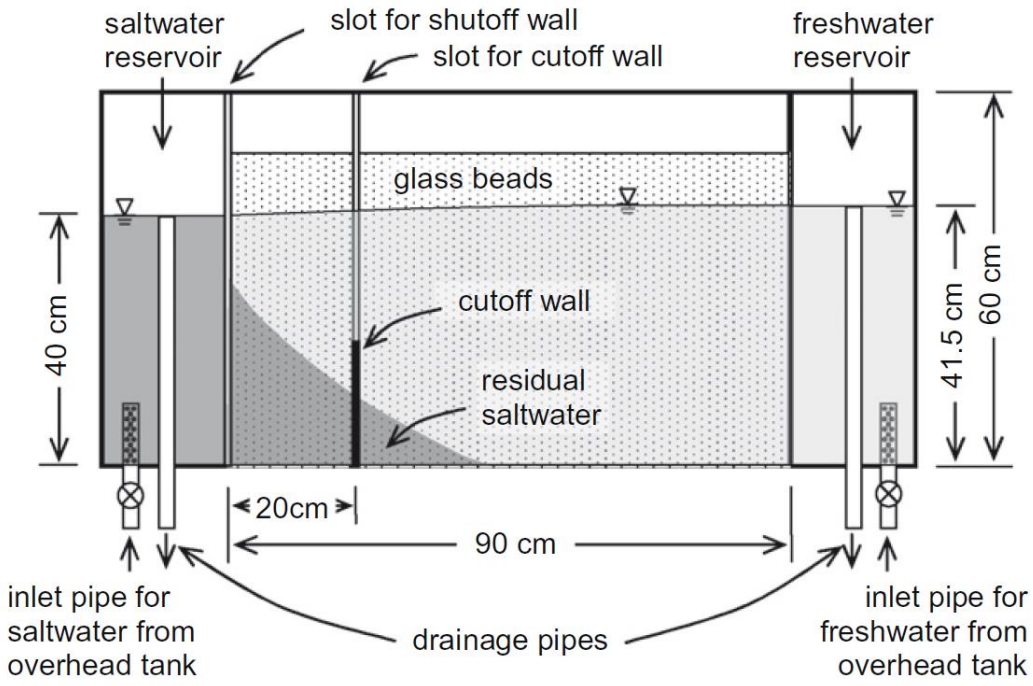

Figure 10 Schematic diagram of the experimental setup.

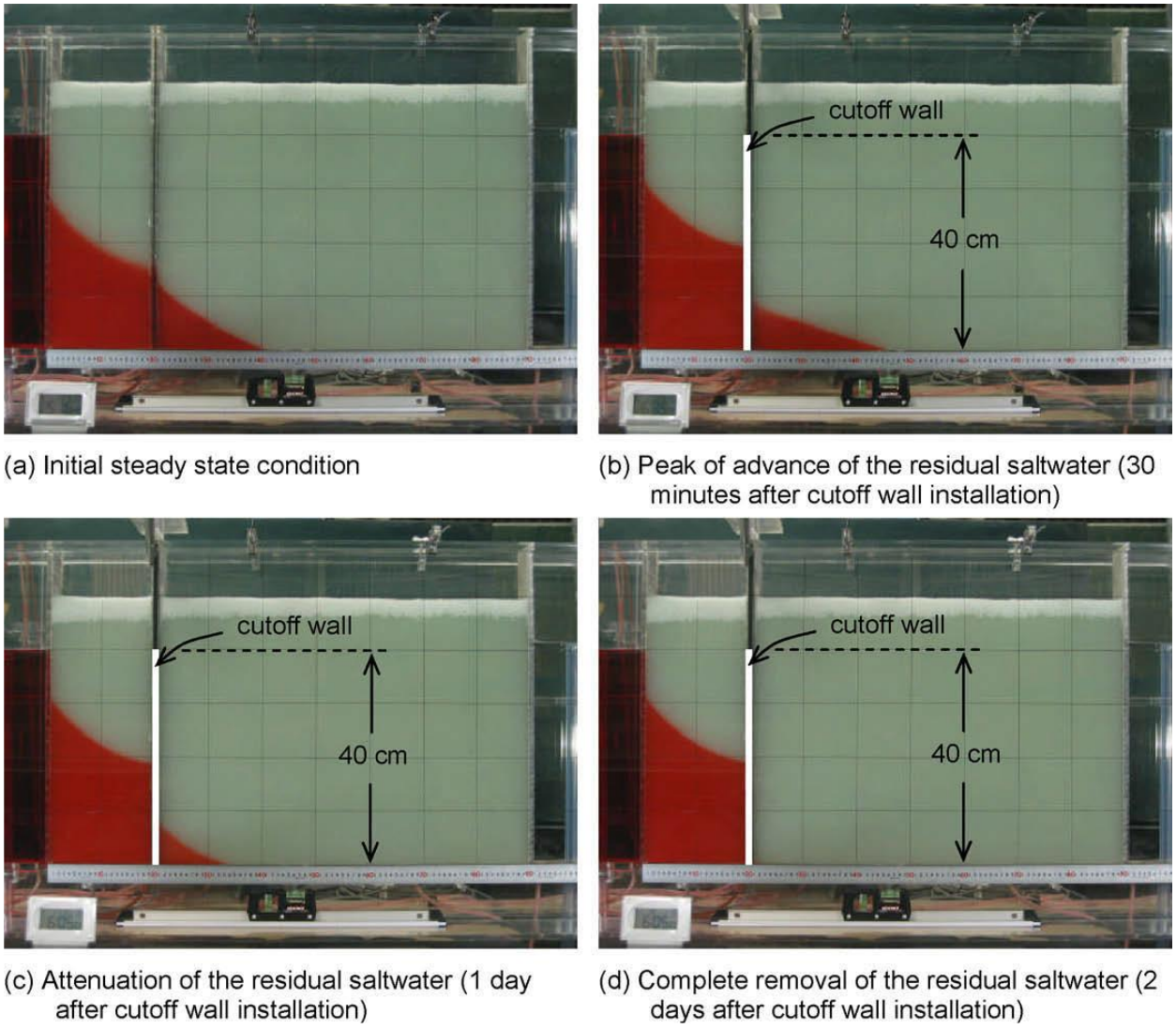

(a) Initial steady state condition

(b) Peak of advance of the residual saltwater (30 minutes after cutoff wall installation)

(c) Attenuation of the residual saltwater (1 day after cutoff wall installation)

(d) Complete removal of the residual saltwater (2 days after cutoff wall installation)

Figure 11 Behavior of the residual saltwater before and after installation of 40-cm cutoff wall

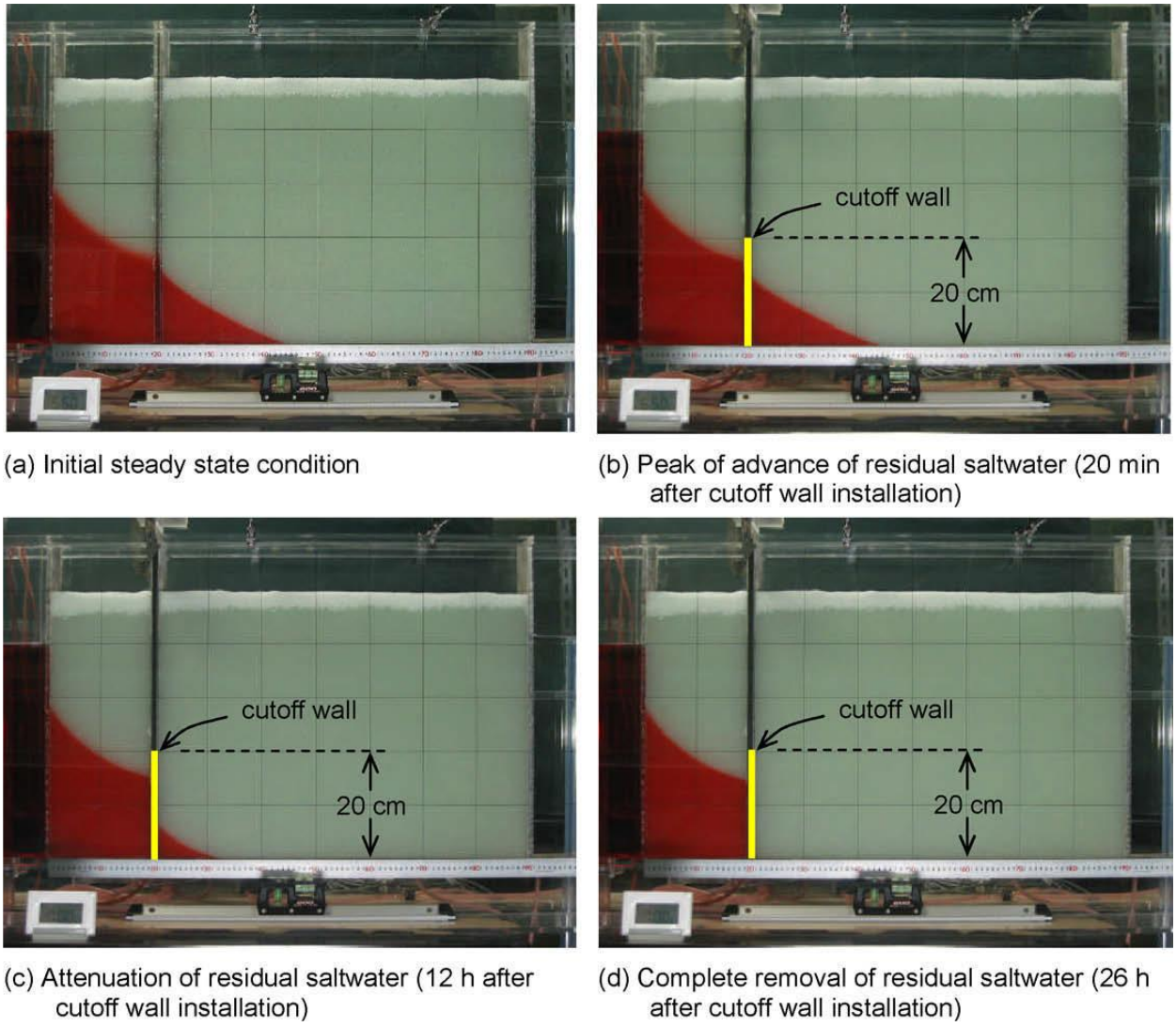

(a) Initial steady state condition

(b) Peak of advance of residual saltwater (20 min after cutoff wall installation)

(c) Attenuation of residual saltwater (12 h after cutoff wall installation)

(d) Complete removal of residual saltwater (26 h after cutoff wall installation)

Figure 12 Behavior of the residual saltwater before and after installation of 20-cm cutoff wall

We conducted experiments and numerical studies to examine the dynamics of residual saltwater after installation of cutoff walls. Experimental results showed that after installation of a cutoff wall, the residual saltwater wedge first flattens, causing the toe to advance, then gradually attenuates and eventually is completely removed from the storage area on the landward side of

the wall. The SEAWAT model adequately predicts the behavior of the advancing saltwater intrusion wedge and the retreating residual saltwater after cutoff wall installation using the transient toe position of the saltwater wedge as point of comparison. Careful analyses of the flow patterns and relative concentration contours from the model enabled us to explain the residual saltwater behavior due to cutoff wall installation. Flow patterns indicated that as freshwater flows along the mixing zone and over the cutoff wall, it transported dispersive flux of salt gradually removing the residual saltwater. Since the inflow of saltwater is prevented, all the residual saltwater was eventually removed from the storage area of the cutoff wall. Our study has proven that saltwater trapped in an enclosing wall would be completely flushed out by the freshwater flow from inland. This phenomenon proves that subsurface dams may be effective not only in preventing saltwater intrusion, but also in reclaiming previously saline-intruded coastal aquifers for freshwater storage and supply.

Recharge channel

The flow domain was discretized using spatially uniform quadratic elements. A mesh-independent solution was obtained with a mesh size of 0.5 centimeters. It should be noted that the SEAWAT is a saturated model, the aquifer was considered as a confined layer in this study, so the created head by recharge canal using the SEEP/W model as boundary condition was inserted into the SEAWAT model. The porous media used by Goswami and Clement (2007) was uniform silica beads of average diameter 1.1 mm with a hydraulic conductivity of 1050 m/day, the porosity of 0.385 and longitudinal and transverse dispersivities considered equal to 1mm and 0.1mm respectively. The relative density of seawater was 1.026 at the reference concentration of 1.0 at the seawater boundary.

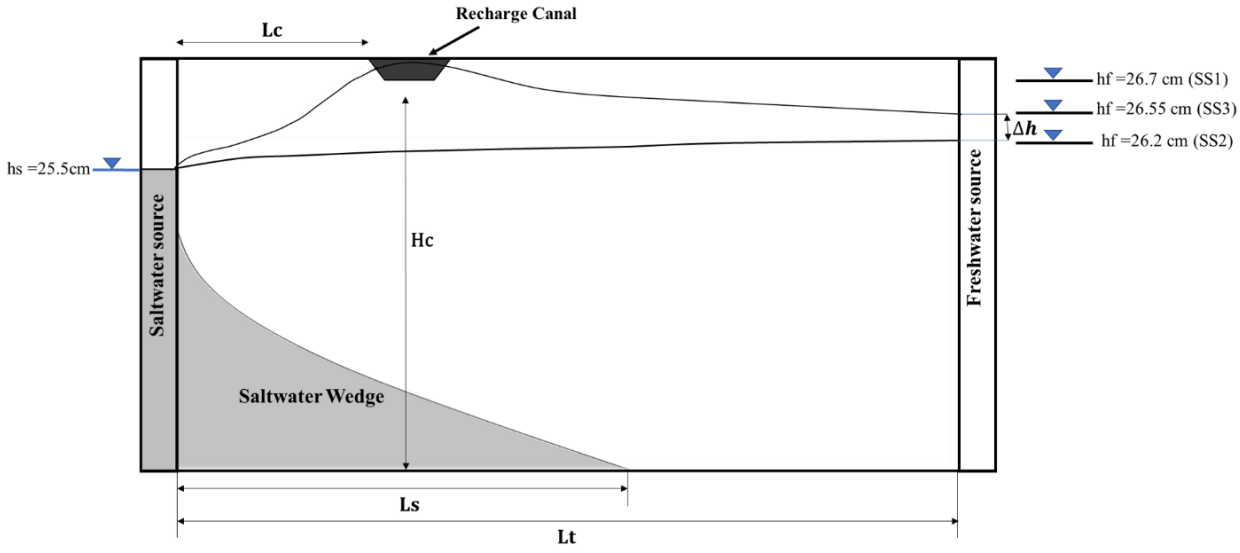

Figure 13 Geometry, boundary conditions used in the numerical model

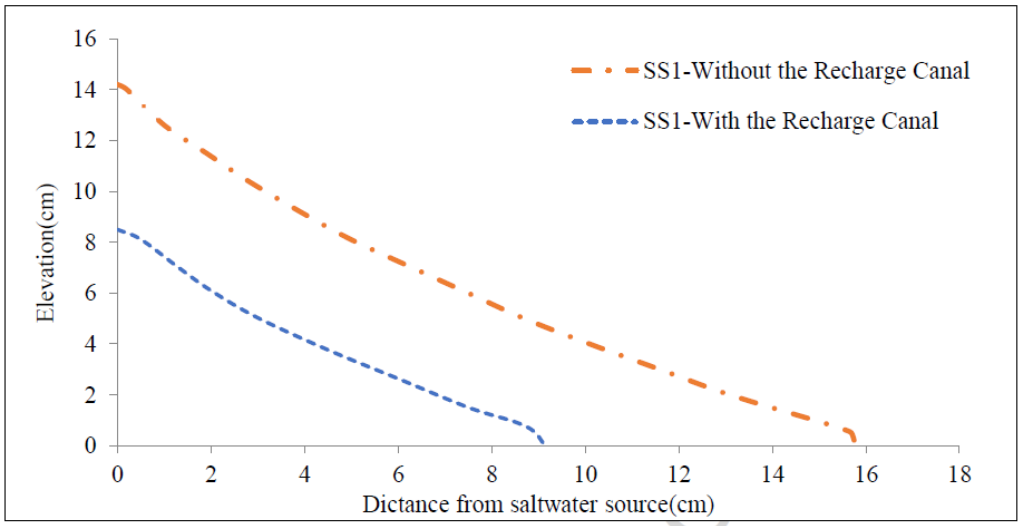

Figure 14 Comparison of fresh-saltwater interface position with and without the recharge canal (the recharge canal is located in its optimal location)

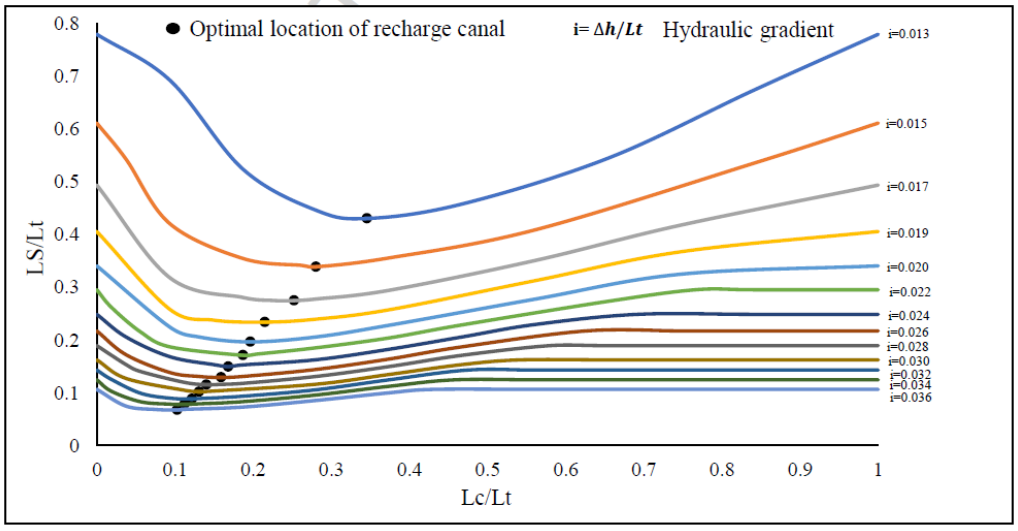

Figure 15 The optimal location of recharge canal for different hydraulic gradients

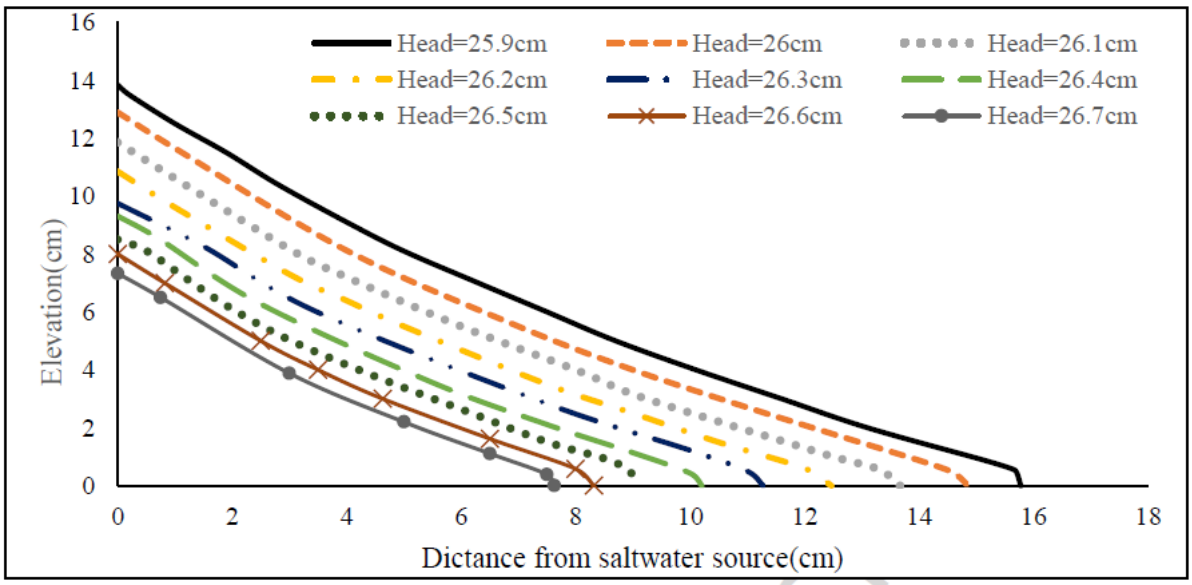

Figure 16 Saltwater wedge position for different water table mound under the canal

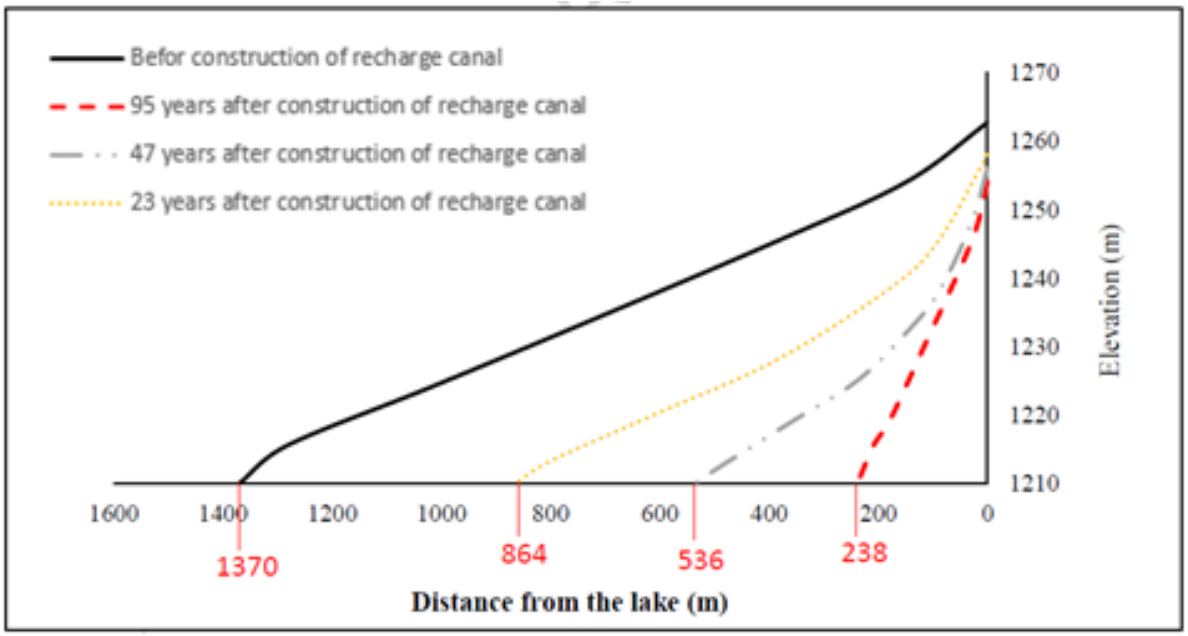

Figure 17 The Saltwater wedge position during the saltwater wedge receding (Lc=1000)

The optimal canal position depends on the toe position of the saltwater wedge, and the relationship between them is almost linear and more effective saltwater repulsion is achieved when the recharge canal is located in the portion near the toe of the saltwater wedge. The recharge canal can result in a recession of the saltwater-wedge between 37 to 45% depending on the hydraulic gradient.

Increasing the water level in the canal increases the elevation of the water table mound under the canal, leading to an increased reduction in the extent of the saltwater intrusion. Consequently, having the ability to control the water level in the recharge canal will provide a greater level of control on saltwater intrusion.

It should be noted that the dimensions of the canal depending on the texture of the soil, the rate of inlet water from the river and the required water recharge rate for making an appropriate water table mound under the canal. The results of the case study showed that a recharge canal with relatively small dimensions could have a significant effect on reduction in the extent of the saltwater intrusion.

References

[1] Mastrocicco, M.; Colombani, N. The Issue of Groundwater Salinization in Coastal Areas of the Mediterranean Region: A Review. Water 2021, 13, 90. https://doi.org/10.3390/w13010090

[2] Li, Fl., Chen, Xq., Liu, Ch. et al. Laboratory tests and numerical simulations on the impact of subsurface barriers to saltwater intrusion. Nat Hazards 91, 1223–1235 (2018). https://doi.org/10.1007/s11069-018-3176-4

[3] Armanuos, A.M., Ibrahim, M.G., Mahmod, W.E. et al. Analysing the Combined Effect of Barrier Wall and Freshwater Injection Countermeasures on Controlling Saltwater Intrusion in Unconfined Coastal Aquifer Systems. Water Resour Manage 33, 1265–1280 (2019). https://doi.org/10.1007/s11269-019-2184-9

[4] Abdelgawad, A.M., Abdoulhalik, A., Ahmed, A.A. et al. Transient Investigation of the Critical Abstraction Rates in Coastal Aquifers: Numerical and Experimental Study. Water Resour Manage 32, 3563–3577 (2018). https://doi.org/10.1007/s11269-018-1988-3

[5] Roger Luyun Jr. a,*,1, Kazuro Momii b, Kei Nakagawa, Laboratory-scale saltwater behavior due to subsurface cutoff wall. Journal of Hydrology 377 (2009) 227–236, DOI: 10.1016/j.jhydrol.2009.08.019

[6] Badaruddin, S., A. D. Werner, and L. K. Morgan (2015), Water table salinization due to seawater intrusion, Water Resour. Res., 51, 8397–8408, doi:10.1002/2015WR017098

[7] Watson, T. A., A. D. Werner, and C. T. Simmons (2010), Transience of seawater intrusion in response to sea level rise, Water Resour. Res., 46, W12533, doi:10.1029/2010WR009564.

[8] M. Motallebian, H. Ahmadi, A. Raoof, et al., An alternative approach to control saltwater intrusion in coastal aquifers using a freshwater surface recharge canal, Journal of Contaminant Hydrology, https://doi.org/10.1016/j.jconhyd.2019.02.007

Climate changes – overview

This report will present projections of climate change for temperature, precipitation and sea level rise from multiple sources. Global, European and Croatian projections for climate changes will be shown. The most relevant sources of information for climate change projections are IPCC (The Intergovernmental Panel on Climate Change) and EEA (The European Environment Agency).

The Intergovernmental Panel on Climate Change (IPCC) is the United Nations body for assessing the science related to climate change. The IPCC was created to provide policymakers with regular scientific assessments on climate change, its implications and potential future risks, as well as to put forward adaptation and mitigation options. [1]

The European Environment Agency (EEA) provides sound, independent information on the environment for those involved in developing, adopting, implementing and evaluating environmental policy, and also the general public. In close collaboration with the European Environmental Information and Observation Network (Eionet) and its 32 member countries, the EEA gathers data and produces assessments on a wide range of topics related to the environment. [2]

IPCC and EEA are explaining climate change projections trough Representative Concentration Pathways (RCPs) and Socioeconomic Pathways (SSPs).

Representative Concentration Pathways (RCPs) have been introduced to climate change research for classifying the stringency of different warming limits. RCPs constitute projections of greenhouse gas emissions and concentrations and their combined radiative forcing. They originally comprised four projections, ranging from RCP 2.6 to RCP 8.5, and after the adoption of the Paris Agreement were augmented by RCP 1.9 to represent mitigation pathways compatible

with the 1.5 °C warming limit. The values refer to radiative forcing in Watt/m2 by the end of the century compared to preindustrial times. [3]

Table 1 Representative Concentration Pathways (RCP) [3]

RCP	Forcing	Temperature	Emission Trend
1.9	1.9 W/m2	~1.5 °C	Very Strongly Declining Emissions
2.6	2.6 W/m2	~2.0 °C	Strongly Declining Emissions
4.5	4.5 W/m2	~2.4 °C	Slowly Declining Emissions
6.0	6.0 W/m2	~2.8 °C	Stabilising Emissions
8.5	8.5 W/m2	~4.3 °C	Rising Emissions

The Shared Socioeconomic Pathways (SSPs) are part of a new framework that the climate change research community has adopted to facilitate the integrated analysis of future climate impacts, vulnerabilities, adaptation and mitigation.

The database includes projections for population (by age, sex, education and urbanization) and economic development (GDP).

In addition to the basic SSP socio-economic elements, the database includes preliminary SSP-based scenarios by integrated assessment models (IAMs). The scenarios provide detailed global and regional projections, among others, for energy supply and use, land-use, GHG and air pollutant emissions, average global radiative forcing and temperature change and mitigation costs. [4]

Projected changes in ground air temperature

Based on EEA, global annual near surface temperature has been rising steadily since the end of the 19th century. The rate of increase has been particularly high since the 1970s at about 0.2°C per decade. In this period, global temperature has risen faster than in any other 50-year period over at least 2000 years, with the past six years (2015–2020) being the warmest on record.

Climate modelling has been used to estimate future climate change for different emissions scenarios and socio-economic pathways underlying these scenarios (Shared Socioeconomic Pathways, SSP). Without significant efforts to curtail emissions, the increase in global temperature will continue rapidly and even accelerate.

Global temperatures are projected to increase by 2.1-3.5°C above pre-industrial levels under SSP2-4.5 and by 3.3-5.7°C under SSP5-8.5 by the end of the 21st century. The only scenarios with a chance to stay within the limits established by the Paris Agreements are SSP1-1.9 with projected warming of 1.0–1.8°C and SSP1-2.6 with ranges between 1.3 to 2.4°C till the end of the 21st century compared to pre-industrial levels. These scenarios assume a drastic reduction in emissions in the coming decades and the decline of CO2 emissions to zero and subsequently negative net emissions around the year 2050 (scenario SSP1-1.9) or around 2080 (scenario SSP1-2.6). [5]

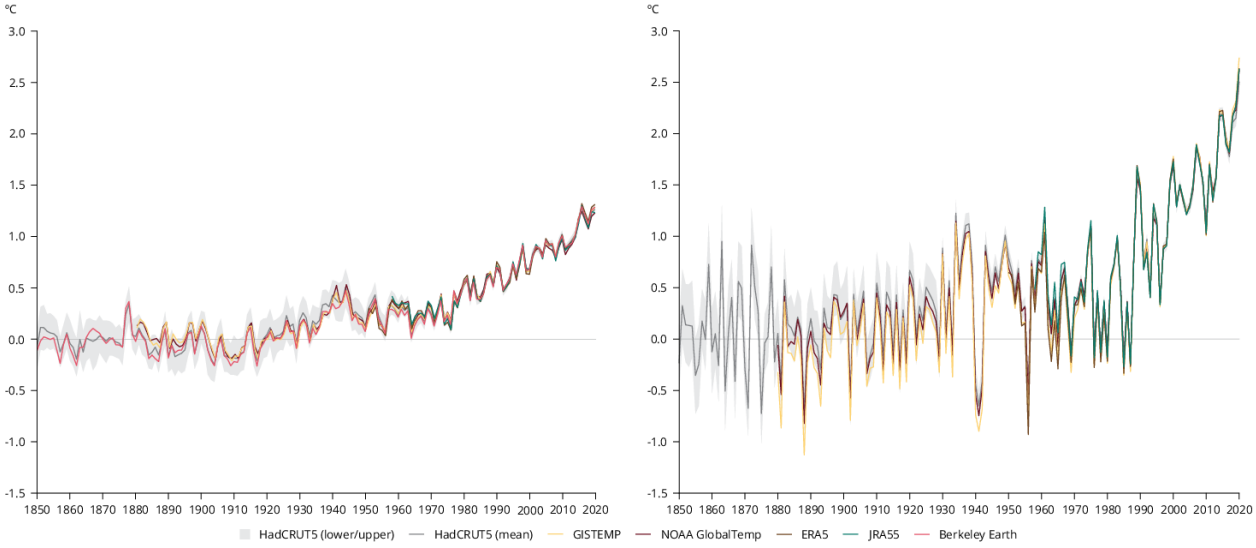

Figure 18 Global (left) and European land (right) average near-surface temperatures anomalies relative to the pre-industrial period [5]

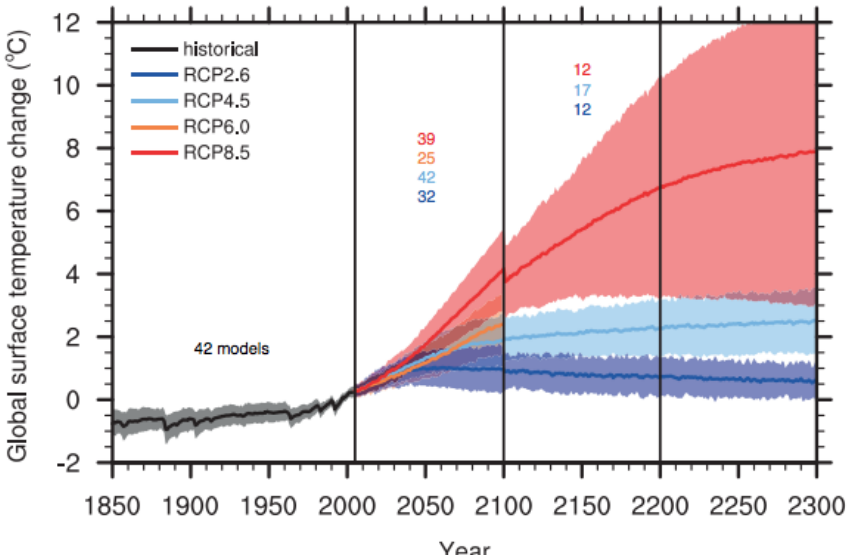

Figure 19 Extended Model Projections of Future Warming Under various IPCC Emissions Scenarios [6]

Europe is warming faster than the global average. The mean annual temperature over European land areas in the last decade was 1.94 to 2.01°C warmer than during the pre-industrial period. The year 2020 was the warmest year in Europe since the instrumental records began according to all datasets used, with the range of anomaly between 2.51°C and 2.74°C above the pre-industrial levels. Particularly high warming has been observed over eastern Europe, Scandinavia and at eastern part of Iberian Peninsula.

Projections from the CMIP6 initiative suggest that temperatures across European land areas will continue to increase throughout this century at a higher rate than the global average. Land temperatures in Europe are projected to increase further by 1.2 to 3.4° under the SSP1-2.6 scenario and by 4.1 to 8.5°C under the SSP5-8.5 scenario (by 2071-2100, compared to 1981–2010). The highest level of warming is projected across north-eastern Europe, northern Scandinavia and inland areas of Mediterranean countries, while the lowest warming is expected in western Europe, especially in the United Kingdom, Ireland, western France, Benelux countries and Denmark. [5]

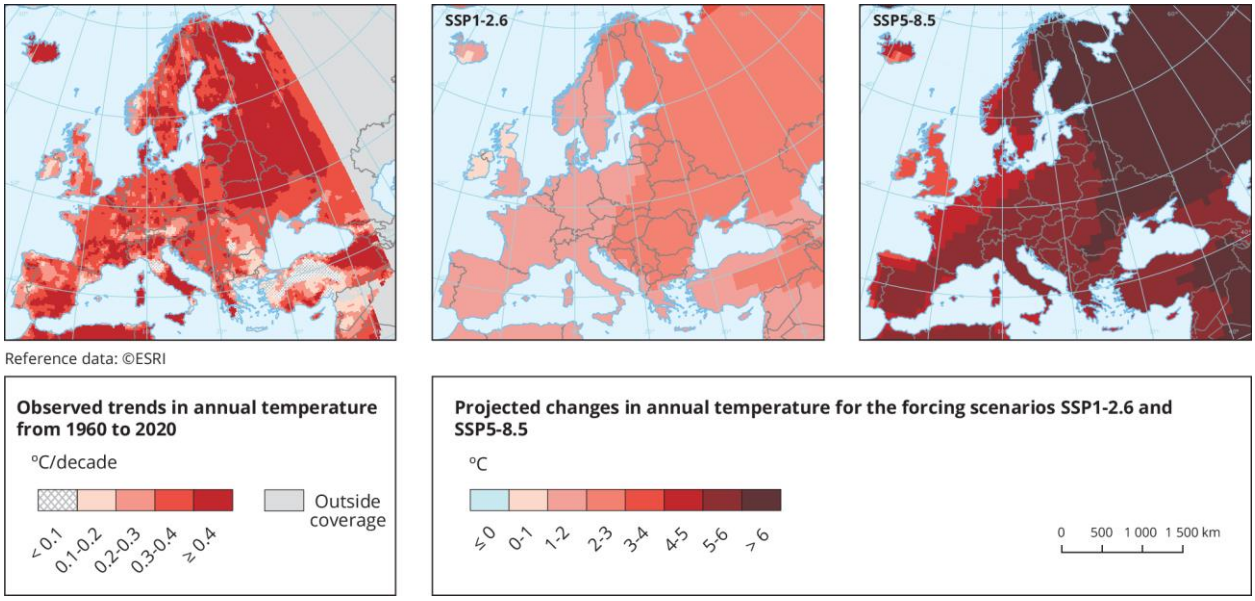

Figure 20 Observed annual mean temperature trend from 1960 to 2020 (left panel) and projected 21st century temperature change under different SSP scenarios (right panels) in Europe [5]

The State Hydrometeorological Institute (DHMZ) uses the regional climate model RegCM [7] from the International Centre for Theoretical Physics in Trieste, Italy. For current climate change simulations, the model takes the initial and boundary conditions from combined global climate model ECHAM5 / MPI-OM [8].

Dynamic adaptation to the RegCM regional model was made for all three implementations of the ECHAM5 / MPI-OM model for two separate periods of current and future climate (time-slice experiment). The current climate is presented in the period 1961-1990, while the future climate according to the A2 scenario is defined in the period 2011-2070. The domain of the regional model covers most of Europe and the Mediterranean area with a spatial step of 35 km. [9]

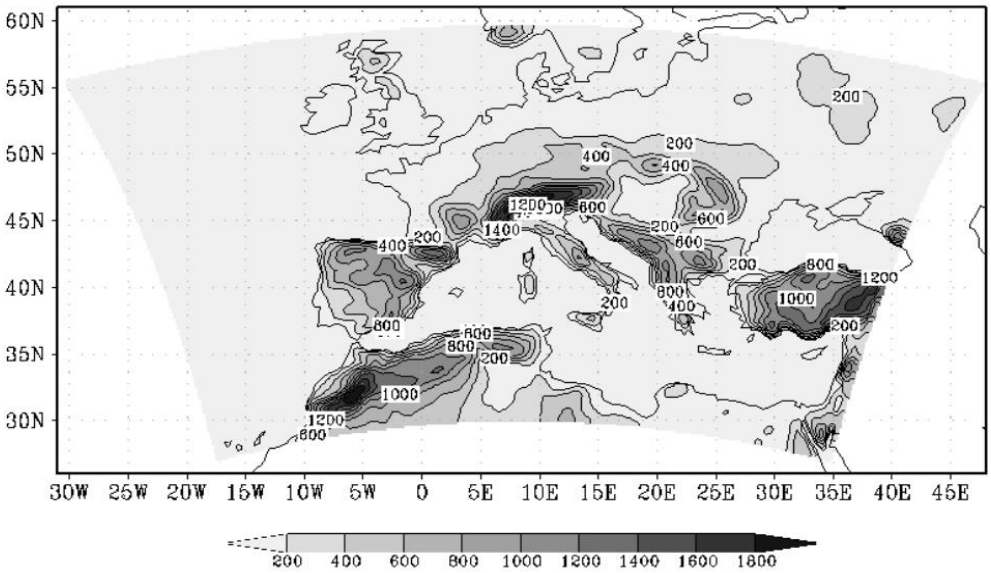

Figure 21 Domain of RegCM model with relief (m) [9]

Future climate changes in Croatia obtained by climate simulations on the regional climate model RegCM according to the A2 scenario were analyzed for two 30-year periods:

1. The period from 2011 to 2040 represents the near future and is of the greatest interest to users of climate information in long-term planning of adaptation to climate change.

2. The period from 2041 to 2070 represents the middle of the 21st century, in which, according to the A2 scenario, a further increase in the concentration of carbon dioxide (CO2) in the atmosphere is predicted and the signal of climate change is stronger.

According to the results of RegCM for Croatian area, the average of the simulation ensemble indicates an increase in air temperature in both periods and in all seasons. The amplitude of the increase is higher in the second than in the first period, but is statistically significant in both

periods. The increase in the average daily air temperature is higher in summer (June - August) than in winter (December - February). [9]

In the first period of the future climate (2011-2040), the temperature in Croatia is expected to rise to 0.6 ° C in winter and to 1 ° C in summer [10].

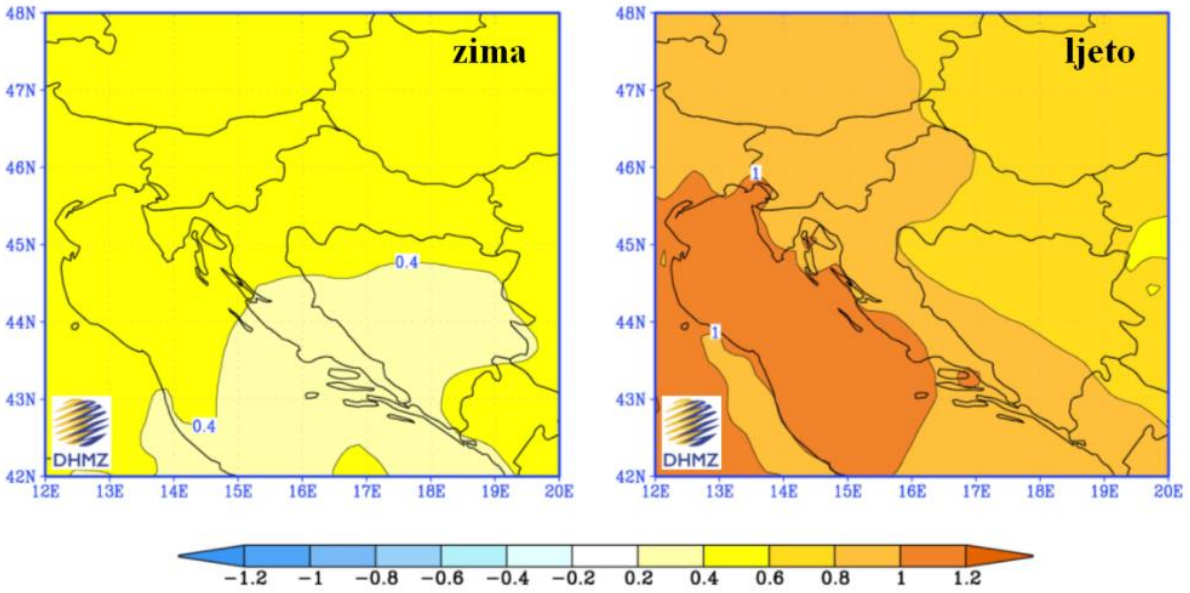

Figure 22 Change in ground air temperature (in ° C) in Croatia in the period 2011-2040 compared to the period 1961-1990 according to the results of the middle class of the RegCM regional climate model ensemble for A2 greenhouse gas emission scenario for winter (left) and summer (right)). [9]

In the second period of the future climate (2041-2070), the expected amplitude of growth in Croatia in winter is up to 2 ° C in the continental part and up to 1.6 ° C in the south, and in summer up to 2.4 ° C in the continental part of Croatia, and up to 3 ° C in the coastal zone [10].

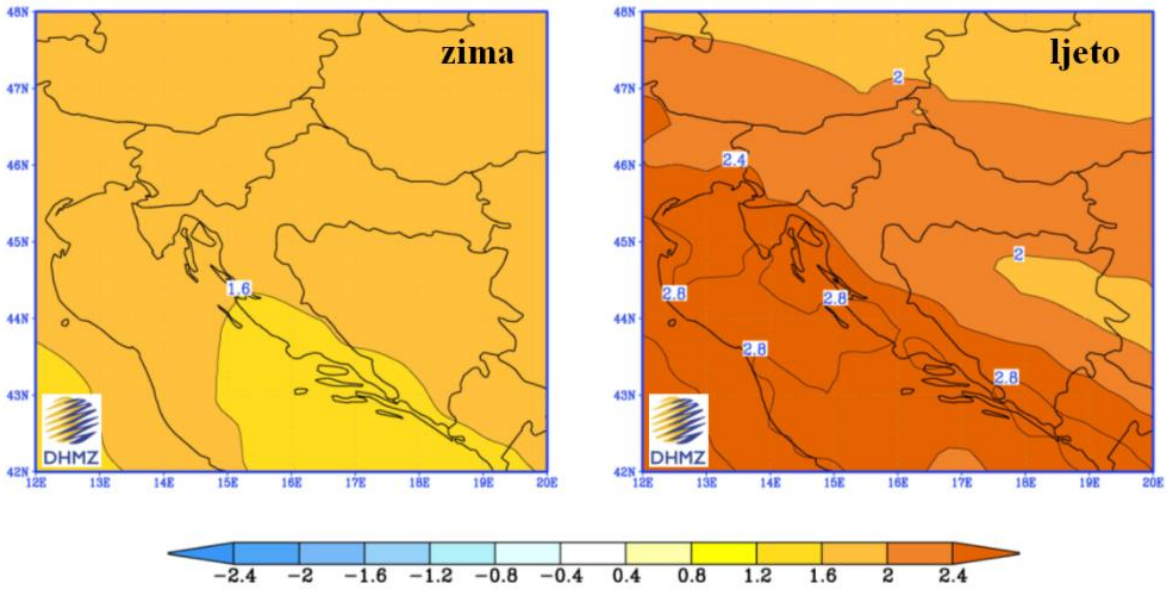

Figure 23 Change in ground air temperature (in ° C) in Croatia in the period 2041-2070 compared to the period 1961-1990 according to the results of the middle class of the RegCM regional climate model ensemble for A2 greenhouse gas emission scenario for winter (left) and summer (right). [9]

The main data source for the World Bank Group's Climate Change Knowledge Portal (CCKP) is the CMIP5 (Coupled Inter-comparison Project No.5) data ensemble. It builds the database for the global climate change projections presented in the Fifth Assessment Report (AR5) of the Intergovernmental Panel on Climate Change (IPCC).

Based on World Bank Group's Climate Change Knowledge Portal (CCKP) Croatia is expected to become hotter and drier, especially in the summer. Climate change trends are projected to increase temperatures and decrease water availability across Croatia over this century. Trends in temperature show warming throughout Croatia, with higher temperatures in the mainland than the coast or the Dalmatian areas. Maximum temperatures are expected to see the greatest degree of change, per decade. CCKP data analysis for high emission scenarios, show monthly

mean temperature changes increasing by 1.36°C by the 2030s to more than 4°C by the 2090s. Temperature trends will see significant increase in summer months (May to September) as well as winter and spring seasons. Minimum temperatures are projected to experience the largest increase through mid-century. Specific 'new hot spots' are in the northern and western areas of Croatia, the northern regions in Gorski Kotar and the eastern part of Lika during its winter months. The coastal areas will experience the biggest change during summer seasons.

Across all emission scenarios, temperatures will continue to increase for Croatia throughout the end of the century. As seen in Figure 24, under a high-emission scenario, average temperatures will increase rapidly by mid-century. Across the seasonal cycle (Figure 25), temperature increases will spike will be felt from April to June and again in September and October. Increased heat and extreme heat conditions will result in significant implications for public, the agricultural sector and water resources. [11]

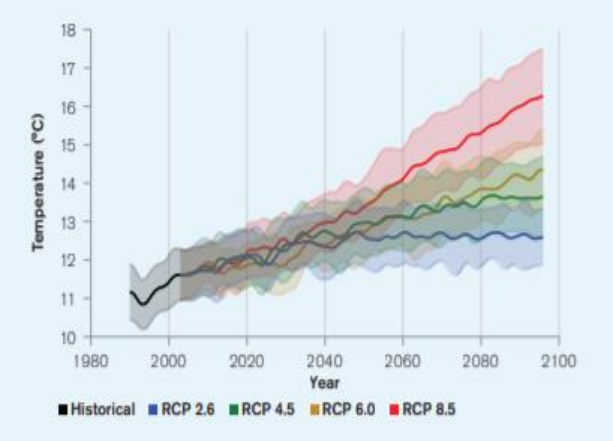

Figure 24 Projected average temperature for Croatia (Reference period 1986-2005) [11]

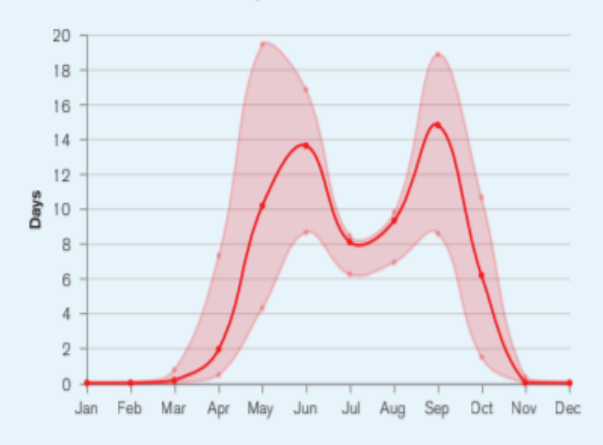

Figure 25 Projected change in summer days (Tmax>25°)(RCP8.5, Ensemble, Reference period 1986-2005) [11]

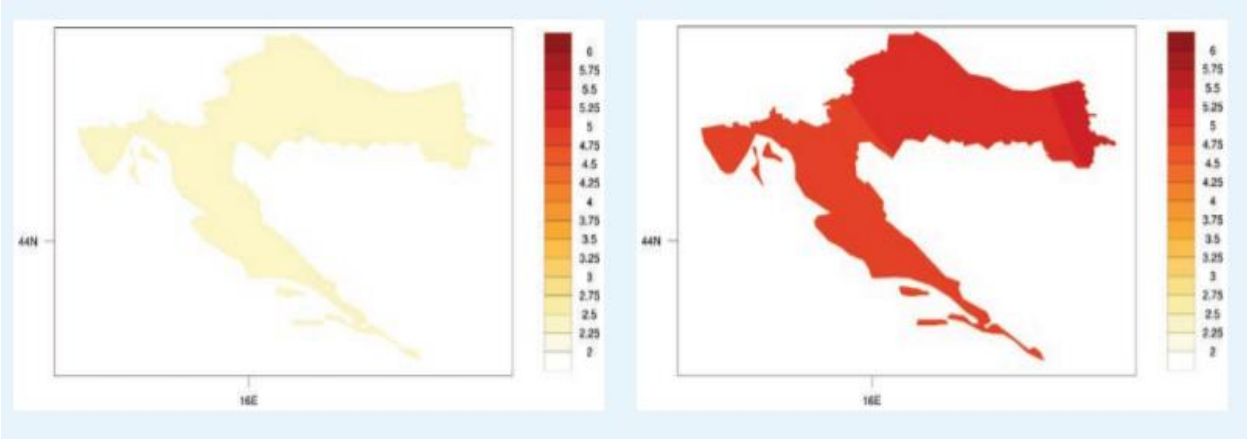

Figure 26 CMIP5 ensemble projected change (32 GCMs) in annual temperature by 2040-2059 (left) and by 2080-2099 (right), relative to 1986-2005 baseline under RCP8.5 [11]

Projected changes in precipitation

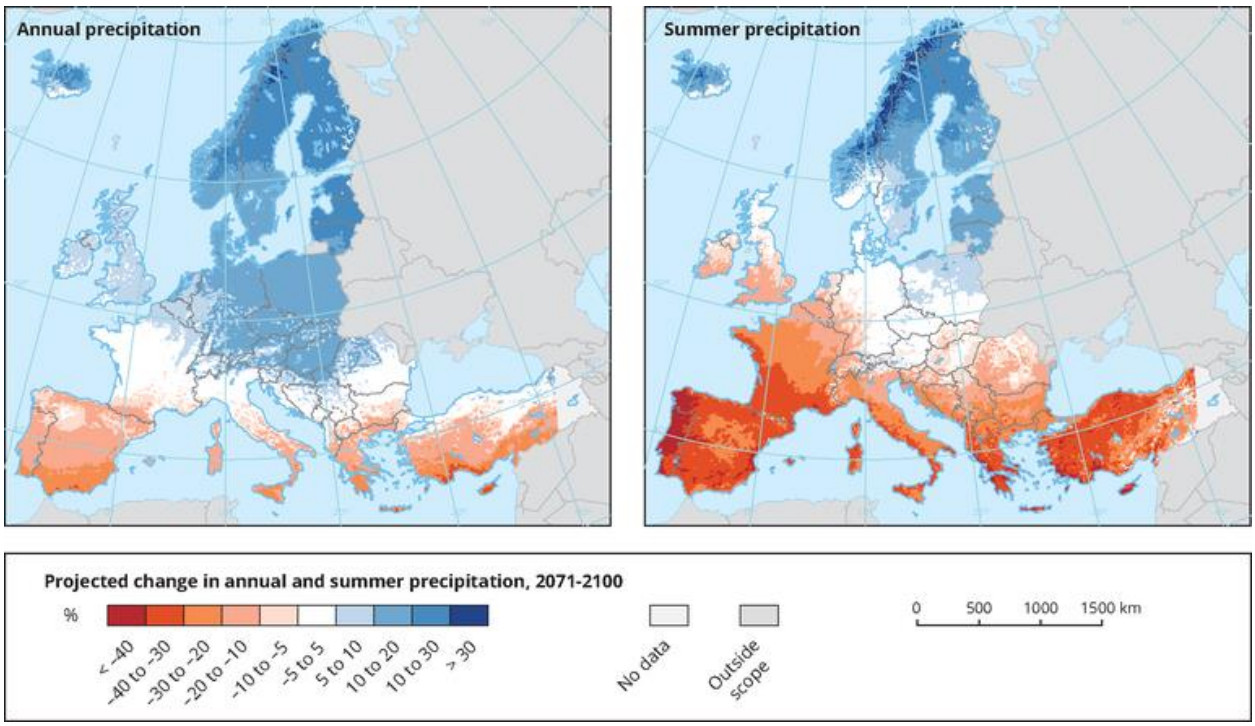

Figure 27 Projected changes in annual (left) and summer (right) precipitation (%) in the period 2071-2100 compared to the baseline period 1971-2000 for the forcing scenario RCP 8.5. Model simulations are based on the multi-model ensemble average of RCM simulations from the EURO-CORDEX initiative. [12]

For a high emissions scenario (RCP8.5), the models project a statistically significant increase in annual precipitation in large parts of central and northern Europe (of up to about 30 %) and a decrease in southern Europe (of up to 40 %) from 1971–2000 to 2071–2100 (Figure 27 left panel). In summer, the precipitation decrease extends northwards (Figure 27 right panel). A zone with small changes that are not significant (but are, however, partially robust in the direction of the change), shows where the precipitation pattern (as presented in the ensemble mean) changes the direction of the change. For a medium emissions scenario (RCP4.5), the magnitude of change is smaller, but the pattern is very similar to the pattern for the RCP8.5 scenarios. The range of

projected changes in precipitation from the multi-model ensemble are generally the same between RCP4.5 and RCP8.5, or larger in RCP8.5, especially at the end of the century. [12]

Based on DHMZ regional climate model, changes in precipitation in the near future (2011-2040) are very small and limited to smaller areas and vary depending on the season. The largest change in precipitation, according to the A2 scenario, can be expected in the Adriatic in the autumn when RegCM indicates a decrease in precipitation with a maximum of approximately 45-50 mm in the southern part of the Adriatic. However, this decrease in the autumn precipitation is not statistically significant. [9]

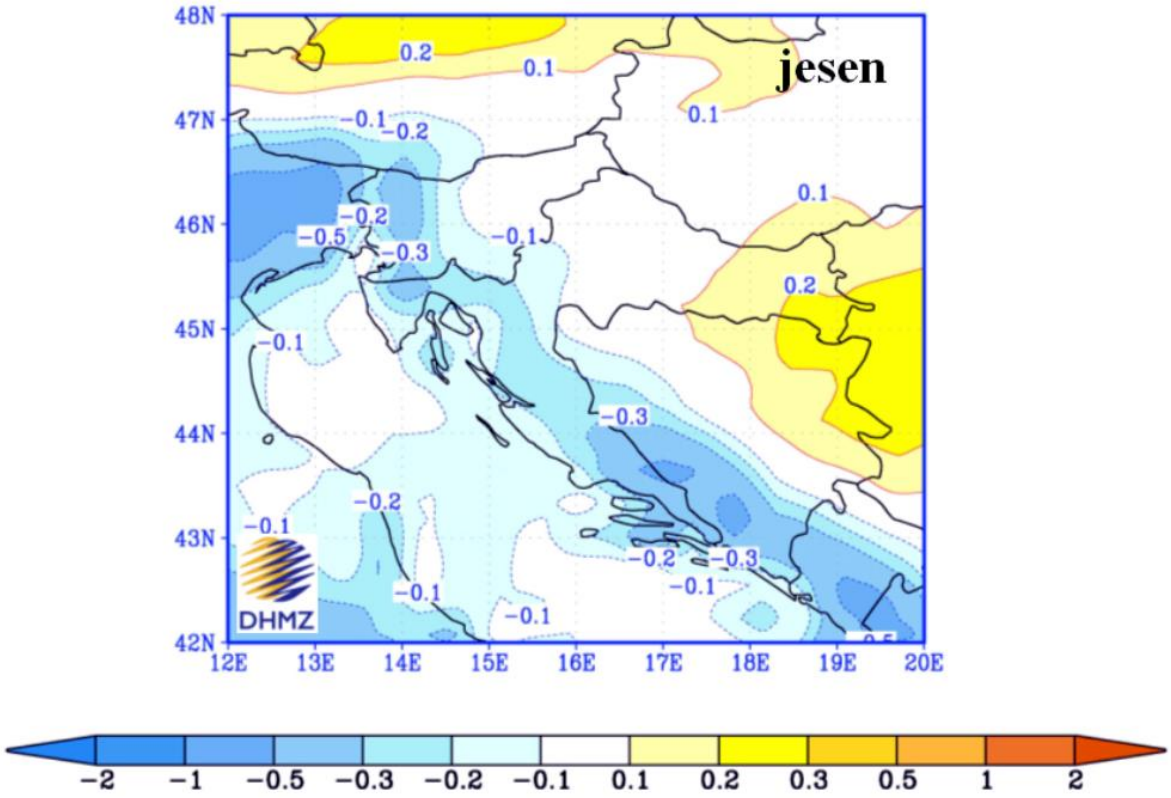

Figure 28 Change in precipitation in Croatia (in mm / day) in the period 2011-2040 compared to the period 1961-1990 according to the results of the regCM regional climate model ensemble for the A2 greenhouse gas emission scenario for autumn. [9]

In the second period of the future climate (2041-2070), precipitation changes in Croatia are more pronounced. Thus, during the summer in mountainous Croatia and in the coastal area, precipitation is expected to decrease. The reductions reach a value of 45 - 50 mm and are statistically significant. In winter, an increase in precipitation can be expected in north-western Croatia and in the Adriatic, but this increase is not statistically significant. [9]

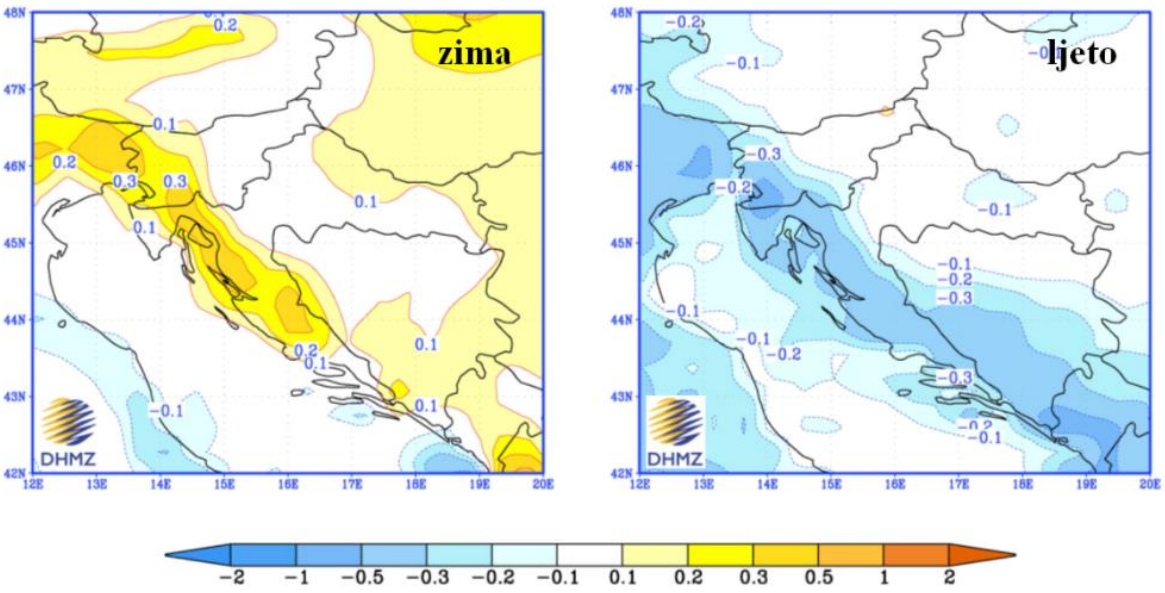

Figure 29 Change in precipitation in Croatia (in mm / day) in the period 2041-2070 compared to the period 1961-1990 according to the results of the middle class of the RegCM regional climate model ensemble for A2 greenhouse gas emission scenario for winter (left) and summer (right). [9]

Based on World Bank Group's Climate Change Knowledge Portal (CCKP) future precipitation trends for Croatia are projected to decline steadily over the century (eastern areas may experience increased rainfall). However, these negative trends are primarily recognized in the summer months in the mountain regions as well as in the Adriatic areas. Annual decreases in precipitation are also expected in Istria and Gorski Kotar, due to reduced spring rainfall. An increased number of consecutive dry days are expected to be seen over the spring season for the northern Adriatic, with summer seasons seeing an extended number of dry days reach the southern coast of Croatia. Through the mid-century, the largest decrease (just over 10 %) will be in the spring in the southern areas of Dalmatia and in the summer (10–15%) in the mountainous areas and in northern Dalmatia. The largest increase in total precipitation, 5–10 %, is expected on the islands in autumn and in northern Croatia in winter. Figure 29 shows the change in the

projected annual average precipitation for Croatia. At a nationally aggregated scale, mean annual precipitation for the country is expected to remain largely similar; however, at regional scales, western and specifically southern areas are expected to experience the most significant reduction in precipitation. [11]

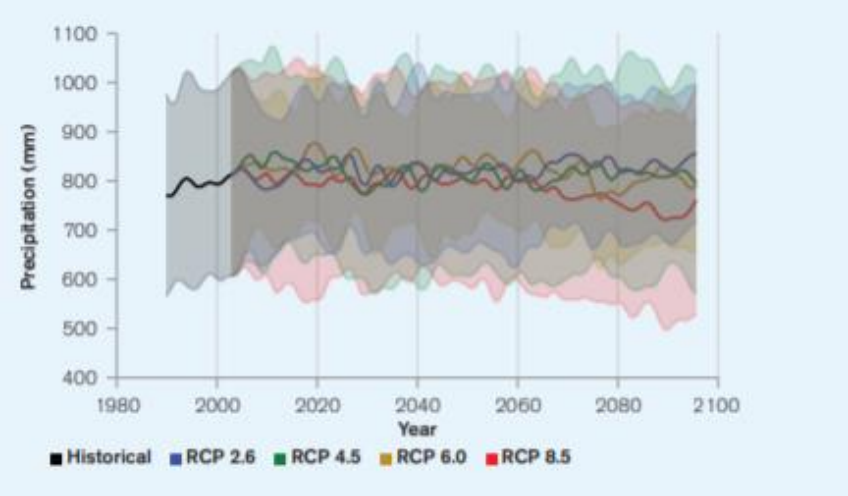

Figure 30 Projected annual average precipitation in Croatia (Reference period 1986-2005) [11]

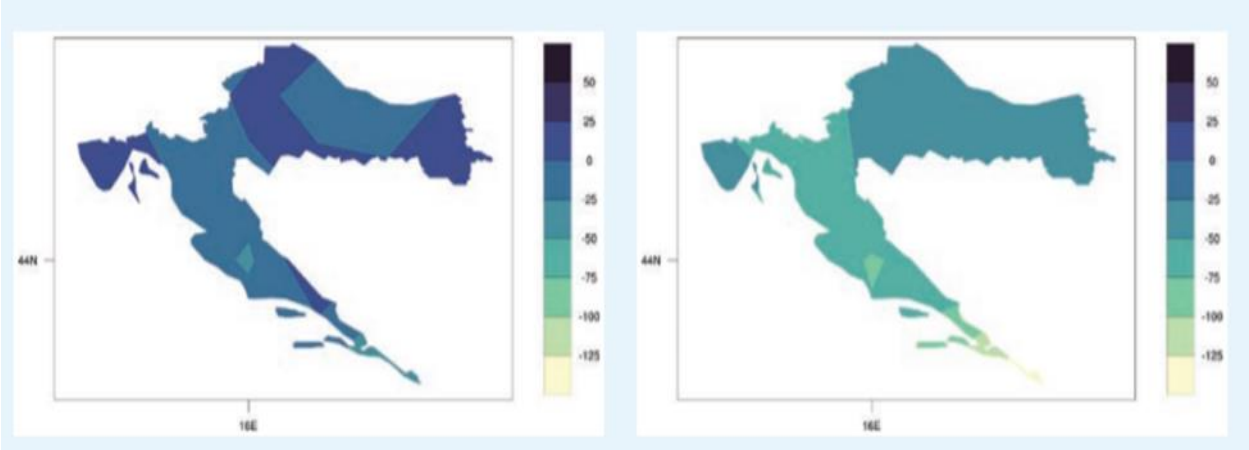

Figure 31 CMIP5 ensemble projected change (32 GCMs) in precipitation (bottom) by 2040-2059 (left) and by 2080-2099 (right), relative to 1986-2005 baseline under RCP8.5 [11]

Projected changes in sea level

Based on EEA global mean sea level (GMSL) has risen about 21 cm since 1900, at an accelerating rate. GMSL reached its highest value ever in 2020. GMSL will likely rise by 0.28-0.55 m under a very low emissions scenario (SSP1-1.9) and 0.63-1.02 m under a very high emissions scenario (SSP5-8.5) by 2100, relative to the 1995-2014 average. GMSL simulations that include the possibility of fast disintegration of the polar ice sheets project a rise of up to 5m by 2150. Most coastal regions in Europe have experienced an increase in sea level relative to land, except for the northern Baltic Sea coast. [13]

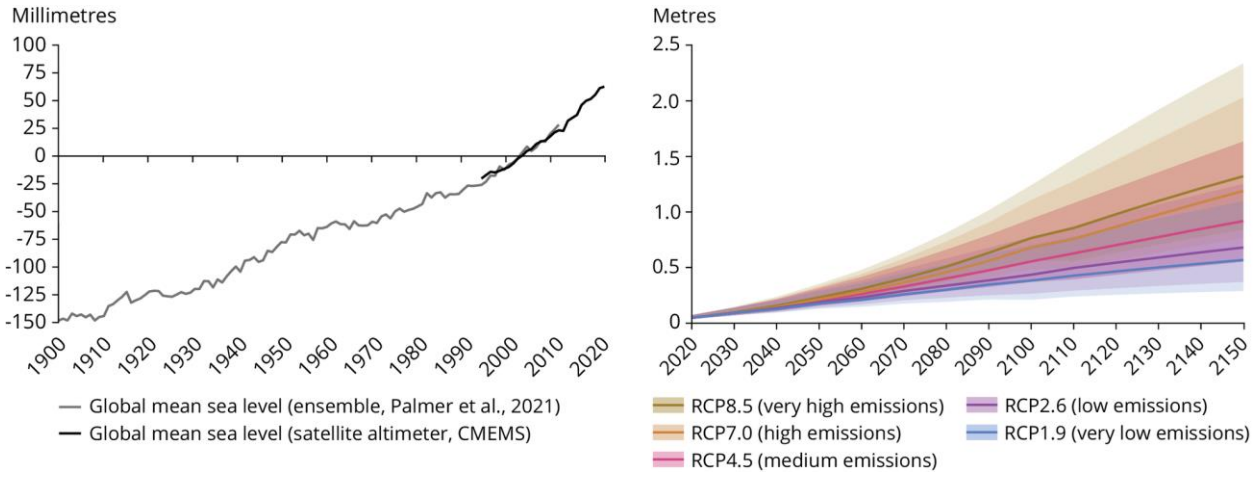

Figure 32 Observed and projected change in global mean sea level [13]

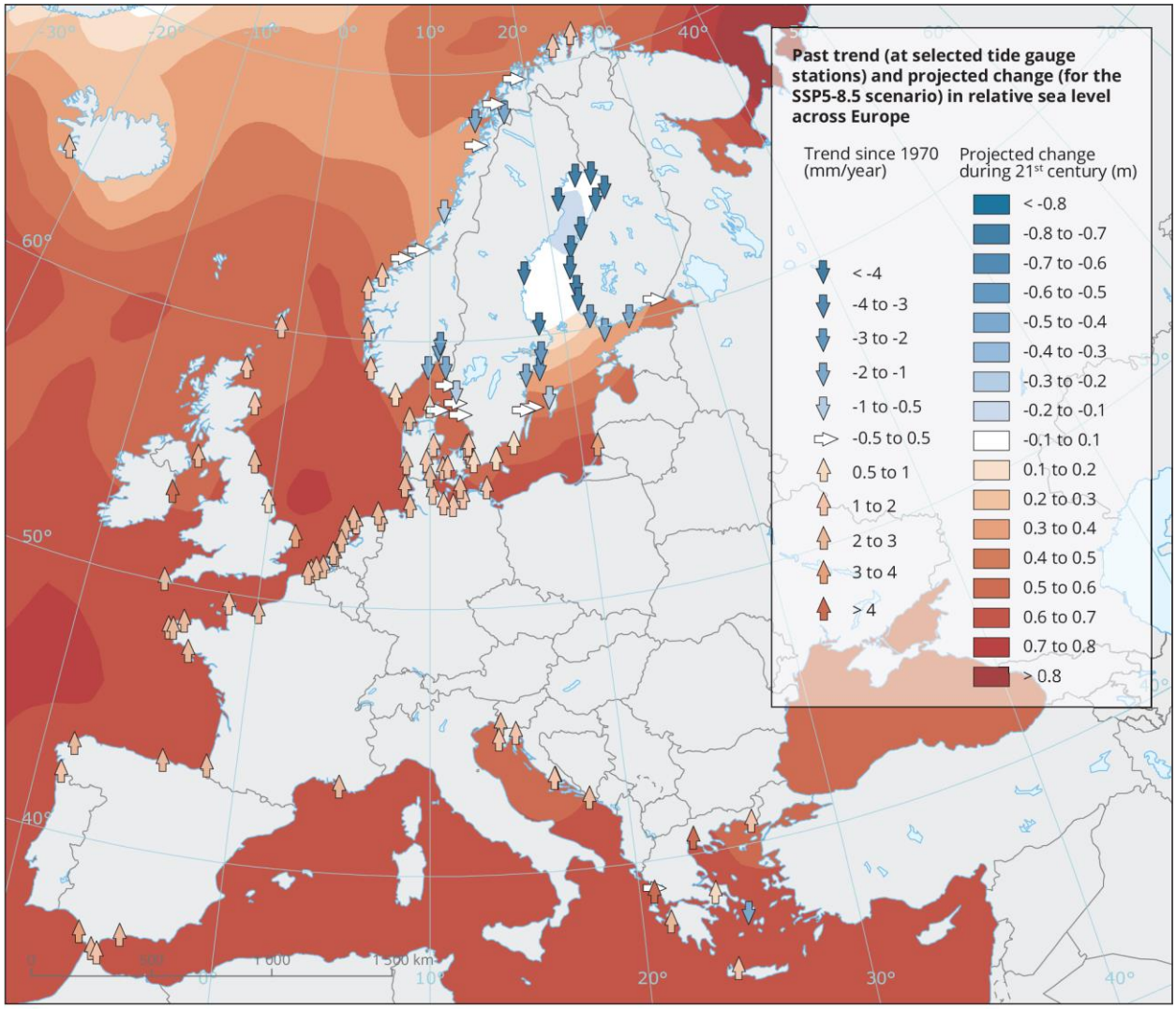

Figure 33 Past trend and projected change in relative sea level across Europe [13]

The IPCC projections of sea level include estimates of contributions from:

- Ocean thermal expansion
- Glacier mass loss
- Greenland and Antarctic ice sheet surface mass balance (net change from the addition of mass through precipitation and loss through melting) and dynamic processes such as collapse of ice shelves
- Changes in land water storage (dams and ground water storage) [14]

Based on IPCC, GMSL will rise between 0.43 m (0.29–0.59 m, RCP2.6) and 0.84 m (0.61–1.10 m, RCP8.5) by 2100 relative to 1986–2005. Beyond 2100, sea level will continue to rise for centuries due to continuing deep ocean heat uptake and mass loss of the GIS and AIS and will remain elevated for thousands of years. Under RCP8.5, the rate of sea level pressure will be 15 mm/yr (10–20 mm/yr) in 2100, and could exceed several cm/yr in the 22nd century. [15]

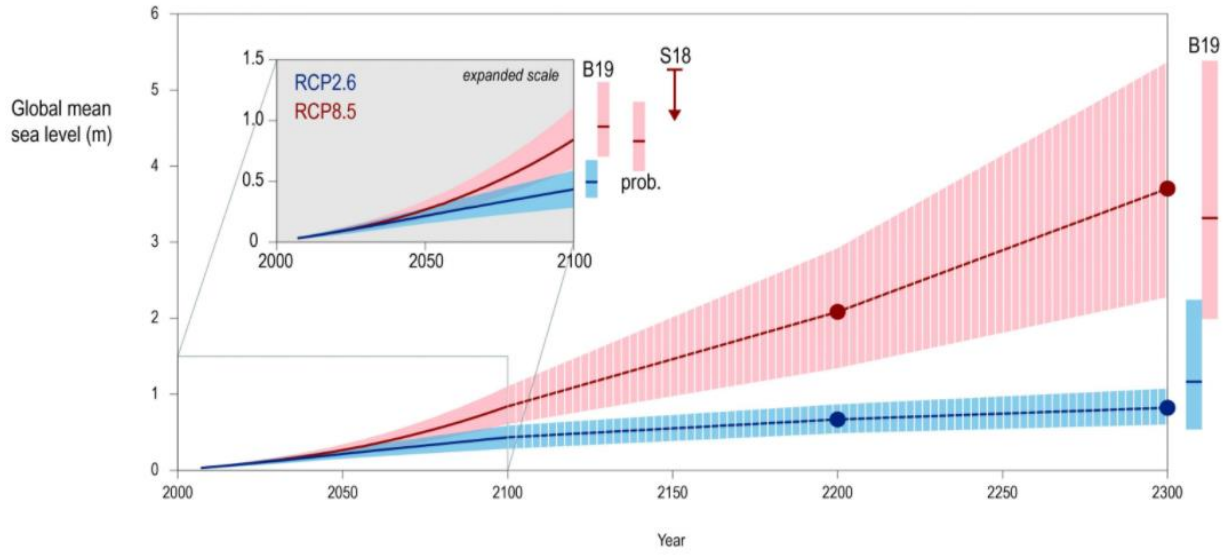

Figure 34 Projected sea level rise (SLR) until 2300 [15]

The inset shows an assessment of the likely range of the projections for RCP2.6 and RCP8.5 up to 2100. Projections for longer time scales are highly uncertain but a range is provided.

In the Republic of Croatia, sea level measurements are carried out at tide gauge stations in Dubrovnik, Split, Zadar, Bakar and Rovinj (Figure 35).

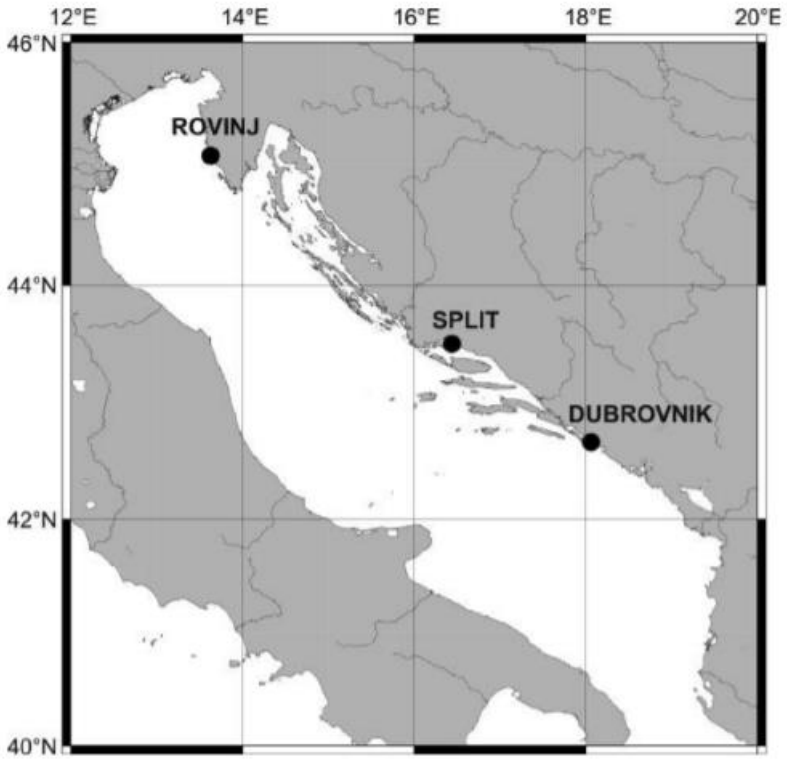

Figure 35 Tide gauge stations in Croatia

The mid-sea level rise test was performed using methods of linear regression analysis. Statistical analysis of average annual values of sea level from 1955 to 2009 indicates a trend of sea level rise from 0.5 to 0.8 mm / year. [16]

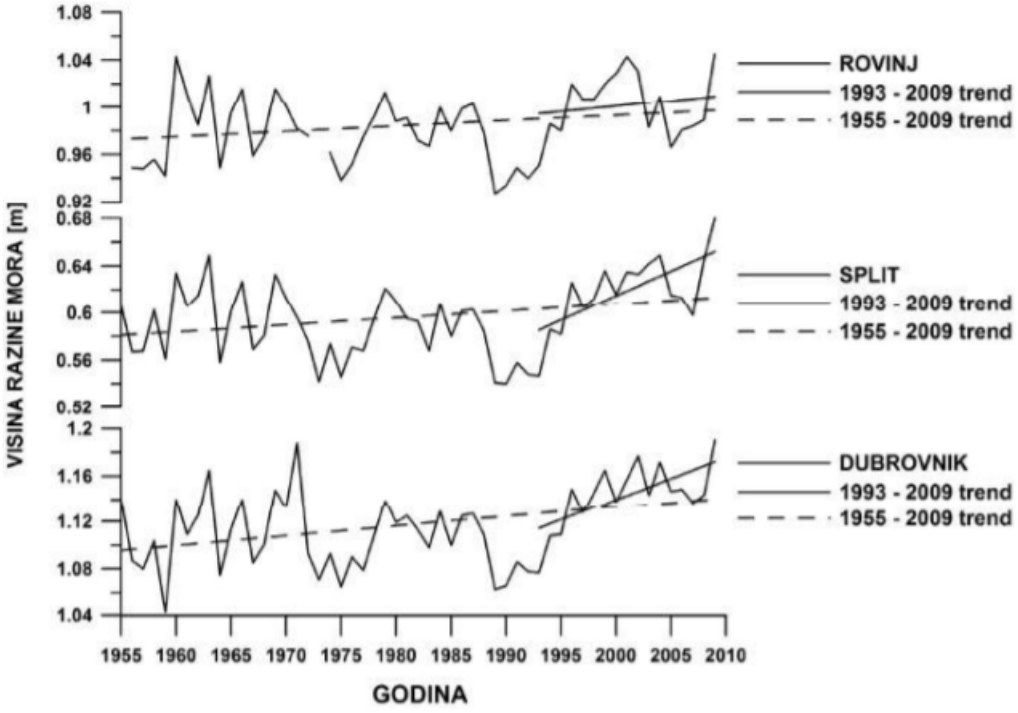

Figure 36 Annual mean sea level values with linear upward trends for Rovinj, Split and Dubrovnik [16]

Analysing the measured values of the mean sea level after 1993, it is possible to observe the trend of accelerated increase of the mean sea level, which is especially pronounced in Split (4.2 mm / year) and Dubrovnik (3.6 mm / year). If this trend continues in the central and southern Adriatic, it would mean an increase in sea level of about 40 cm over the next hundred years, which is in line with IPCC forecasts, which estimate that global sea level rise from 2000 to 2100 is between 20 and 50 cm. [16]

References

[1] https://www.ipcc.ch/.

[2] https://www.eea.europa.eu/.

[3] https://climatescenarios.org/primer/mitigation/.

[4] https://secure.iiasa.ac.at/web-apps/ene/SspDb/dsd?Action=htmlpage&page=about.

[5] https://www.eea.europa.eu/ims/global-and-european-temperatures.

[6] M. e. a. Collins, «Long-term Climate Change: Projections, Commitments and Irreversibility, » Climate Change 2013: The Physical Science Basis, 2013.

[7] P. J. e. al., «Regional climate modeling for the developing world: The ICTP RegCM3 and RegCNET,» Bulletin of the American Meteorological Society, vol. 88, pp. 1395-1409, 2007.

[8] R. E. e. al., «The atmospheric general circulation model ECHAM5. Part I: model description, » Max-Planck Institute for Meteorology, Hamburg, 2003.

[9] https://meteo.hr/klima.php?section=klima_modeli&param=klima_promjene.

[10] Č. Branković, I. Güttler, M. Patarčić e L. Srnec, «Climate Change Impacts and Adaptation Measures - Climate Change scenario,» Fifth National Communication of the Republic of Croatia under the United Nation Framework Convention on the Climate Change, Ministry of Environmental Protection, Physical Planning and Construction, 2010.

[11] Bank, The World Bank Group, «Climate Risk Profile: Croatia, » 2021.

[12] https://www.eea.europa.eu/data-and-maps/figures/projected-changes-in-annual-and-5.

[13] https://www.eea.europa.eu/ims/global-and-european-sea-level-rise.

[14] https://research.csiro.au/slrwavescoast/sea-level/future-sea-level-changes/.

[15] https://www.ipcc.ch/srocc/chapter/chapter-4-sea-level-rise-and-implications-for-low-lying-islands-coasts-and-communities/.

[16] e. a. Srđan Č., «Klimatske promjene, porast razine mora na Hrvatskoj obali Jadrana?,» in 5. Hrvatska konferencija o vodama, Opatija, 2011.

Mitigation measures for the sea water intrusion in coastal systems

Active intrusion

There are two main directions of the sea water intrusion within the Neretva coastal aquifer system:

- Adriatic Sea which creates a western border of the Neretva coastal aquifer system and causes main source of the sea water intruding this coastal aquifer during the year;
- River Neretva bed which represents second dominant source of the seawater during the dry season. This season takes 5-7 months depending on the local hydrological and meteorological conditions.

Measurements of the river Neretva EC (Figure 37 and Figure 38) enable the insight to the fact more than 60% of the Neretva water column represents the sea water during the dry period.

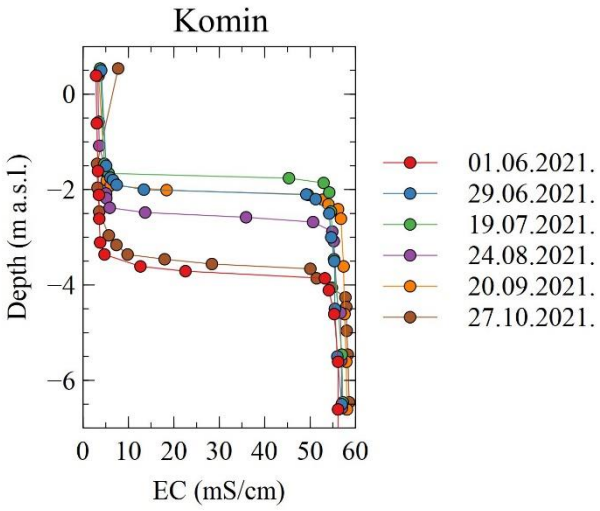

Figure 37 EC profiles of the Neretva water column at Komin profile performed during 2021

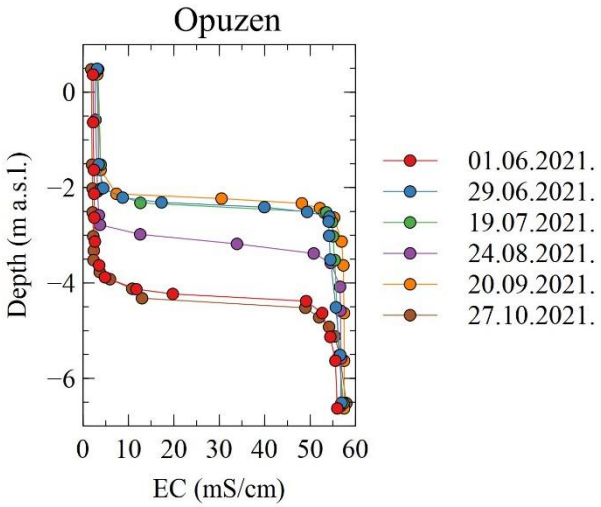

Figure 38 EC profiles of the Neretva water column at Opuzen profile performed during 2021

To perform analysis of the sea water cline in active conditions along the Neretva coastal area, a number of laboratory experiments have been performed. To include climate change scenarios, sea water and inland water levels changes have been performed. In this way, climate changes of sea water elevation change, inland water change due to the precipitation and evapotranspiration changes have been performed.

For this purpose, natural conditions of the active sea water cline have been demonstrated for different gradients in Figure 39 to Figure 48 and Figure 49 to Figure 53.

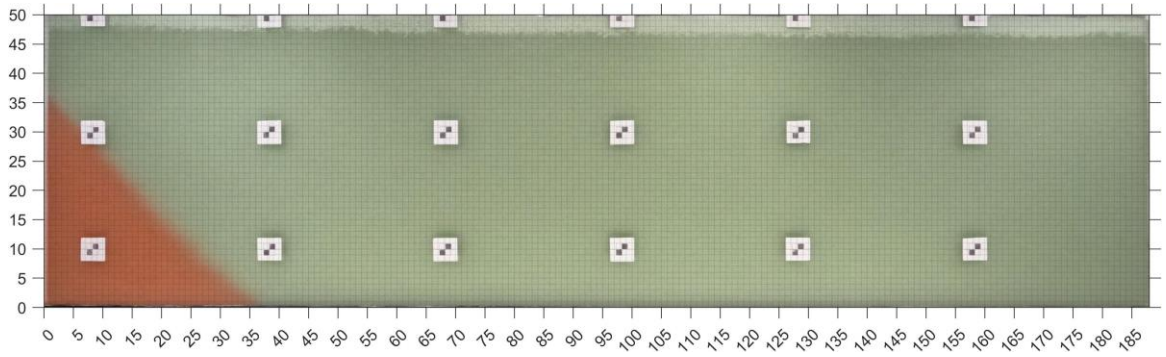

Figure 39 Sea water cline at t= 10 min for the active intrusion hSEA = 40 cm; hINLAND=39 cm

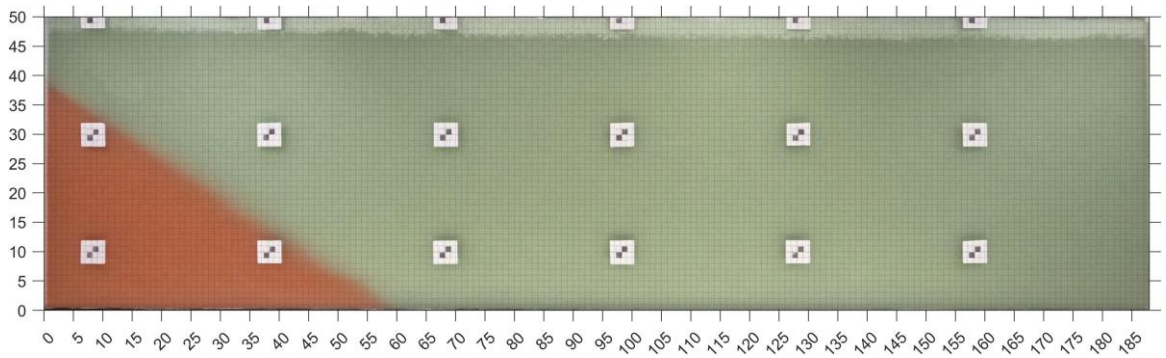

Figure 40 Sea water cline at t= 20 min for the active intrusion hSEA = 40 cm; hINLAND=39 cm

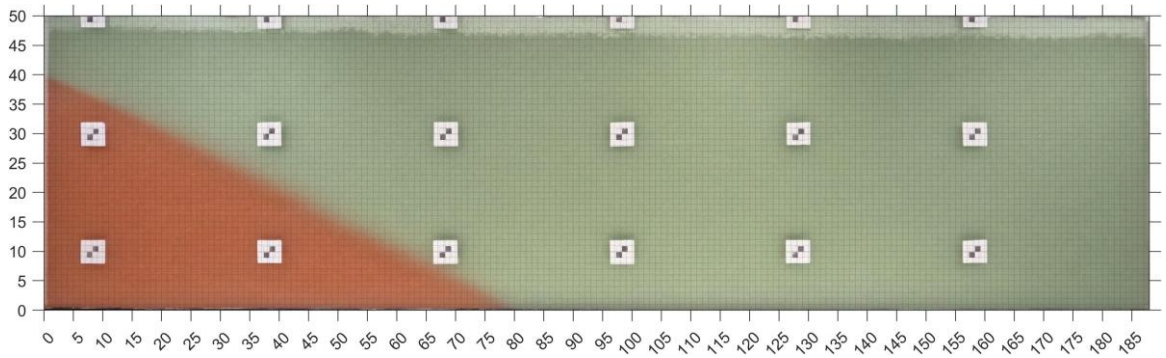

Figure 41 Sea water cline at t= 30 min for the active intrusion hSEA = 40 cm;hINLAND=39 cm

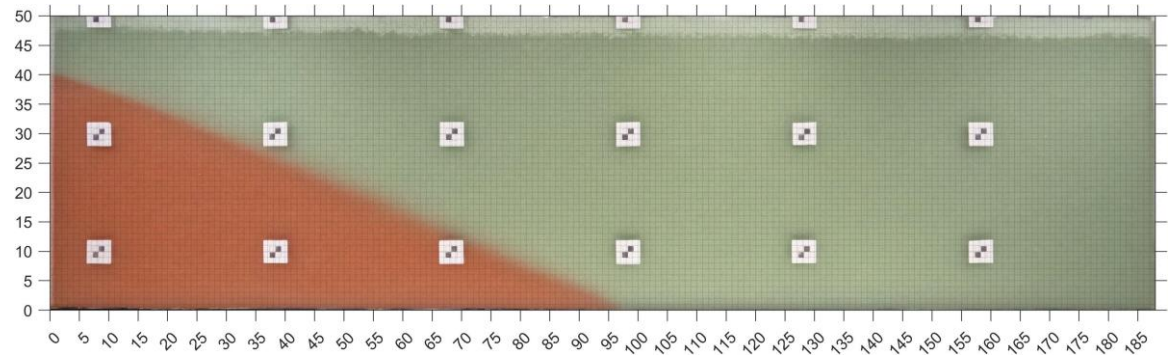

Figure 42 Sea water cline at t= 40 min for the active intrusion hSEA = 40 cm;hINLAND=39 cm

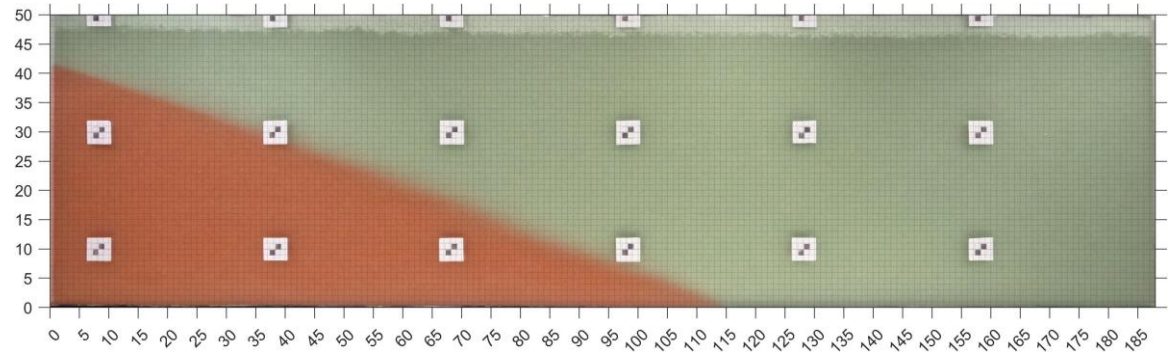

Figure 43 Sea water cline at t= 50 min for the active intrusion hSEA = 40 cm;hINLAND=39 cm

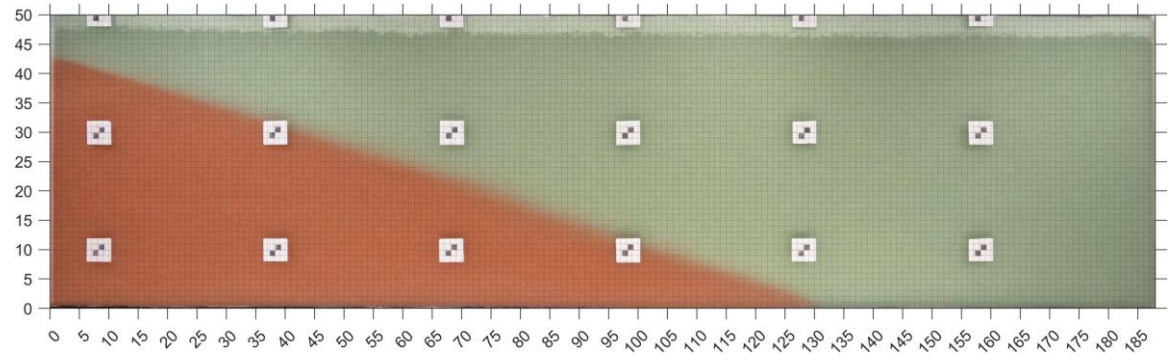

Figure 44 Sea water cline at t= 60 min for the active intrusion hSEA = 40 cm;hINLAND=39 cm

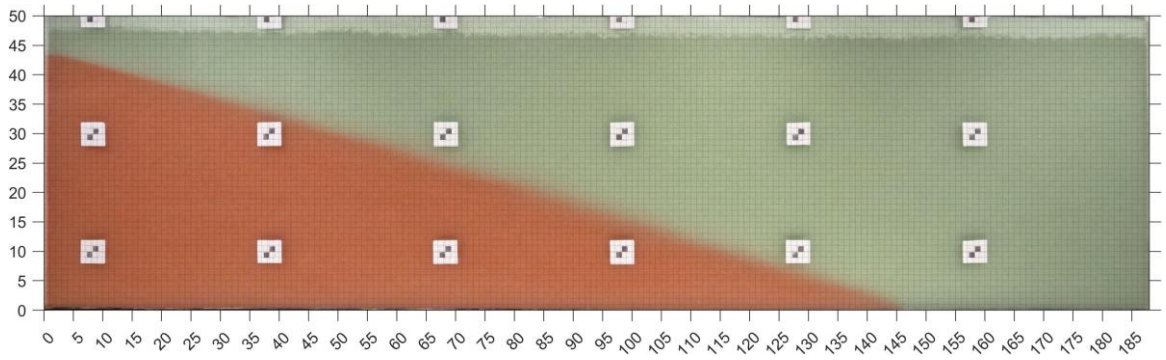

Figure 45 Sea water cline at t= 70 min for the active intrusion hSEA = 40 cm;hINLAND=39 cm

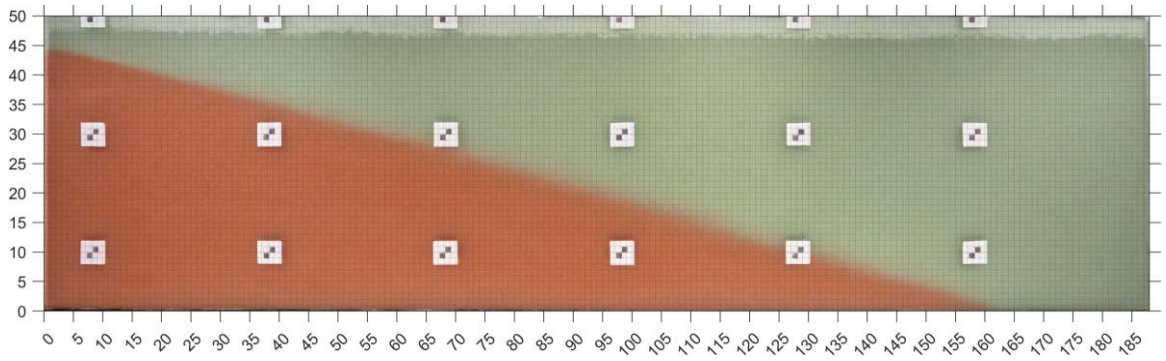

Figure 46 Sea water cline at t= 80 min for the active intrusion hSEA = 40 cm;hINLAND=39 cm

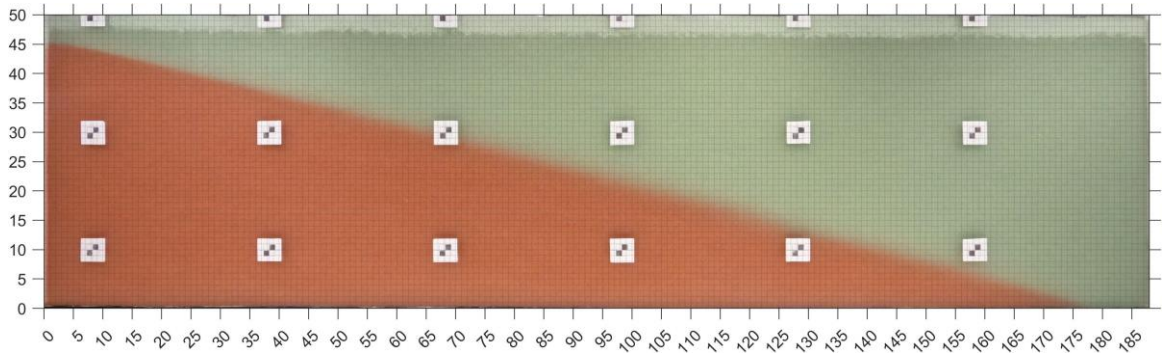

Figure 47 Sea water cline at t= 90 min for the active intrusion hSEA = 40 cm;hINLAND=39 cm

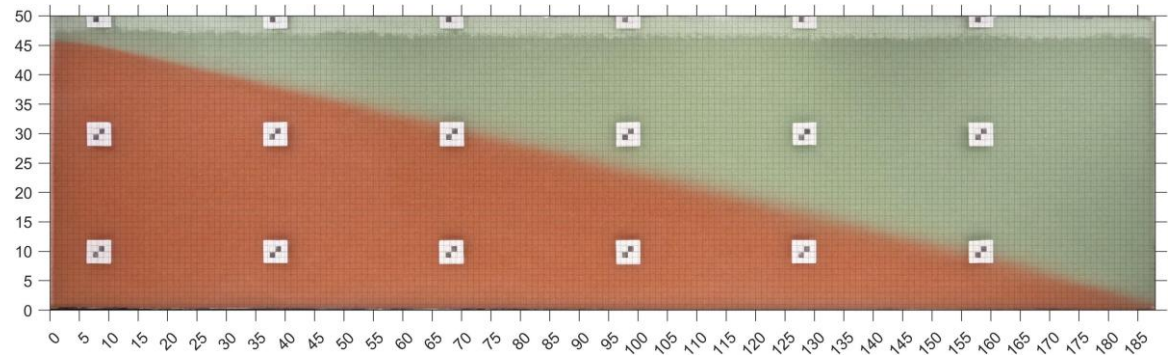

Figure 48 Sea water cline at t= 100 min for the active intrusion hSEA = 40 cm;hINLAND=39 cm

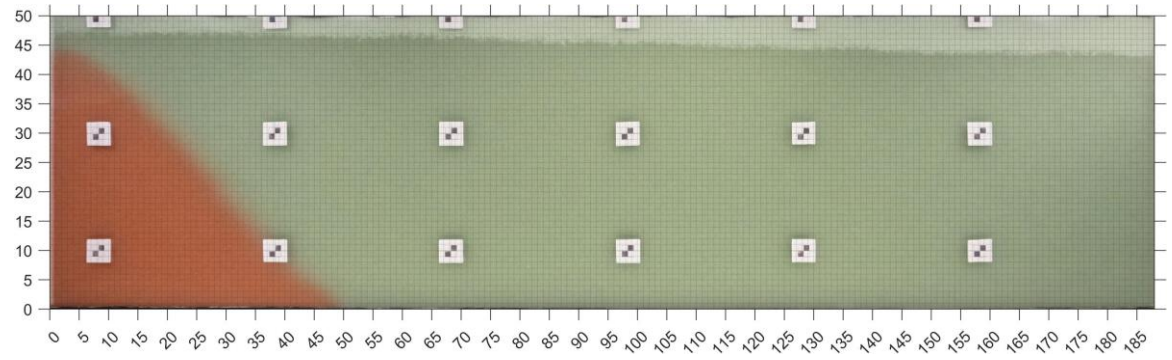

Figure 49 Sea water cline at t= 10 min for the active intrusion hSEA = 40 cm;hINLAND=36 cm

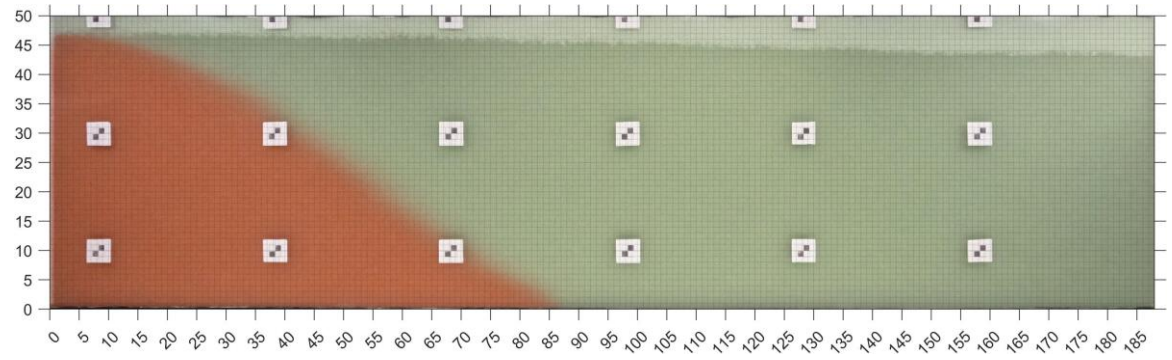

Figure 50 Sea water cline at t= 20 min for the active intrusion hSEA = 40 cm;hINLAND=36 cm

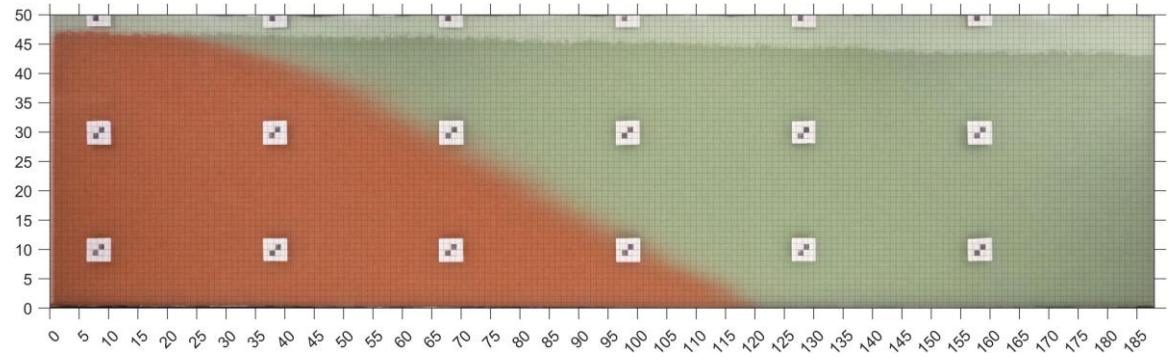

Figure 51 Sea water cline at t= 30 min for the active intrusion hSEA = 40 cm;hINLAND=36 cm

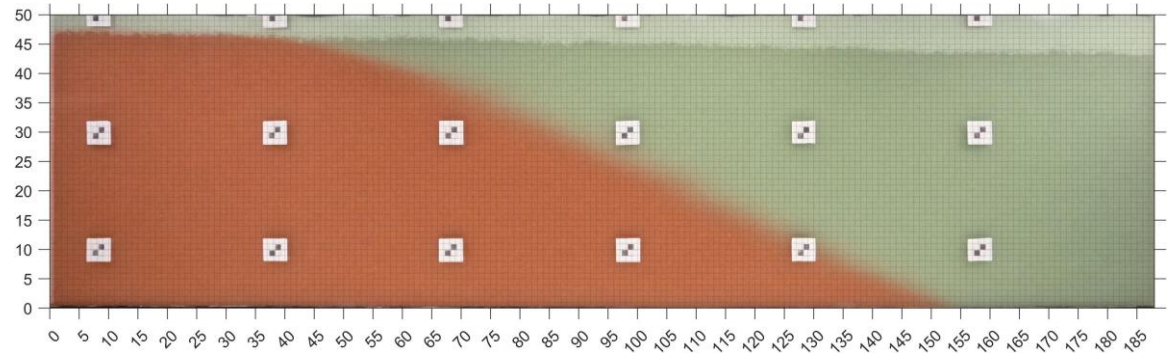

Figure 52 Sea water cline at t= 40 min for the active intrusion hSEA = 40 cm;hINLAND=36 cm

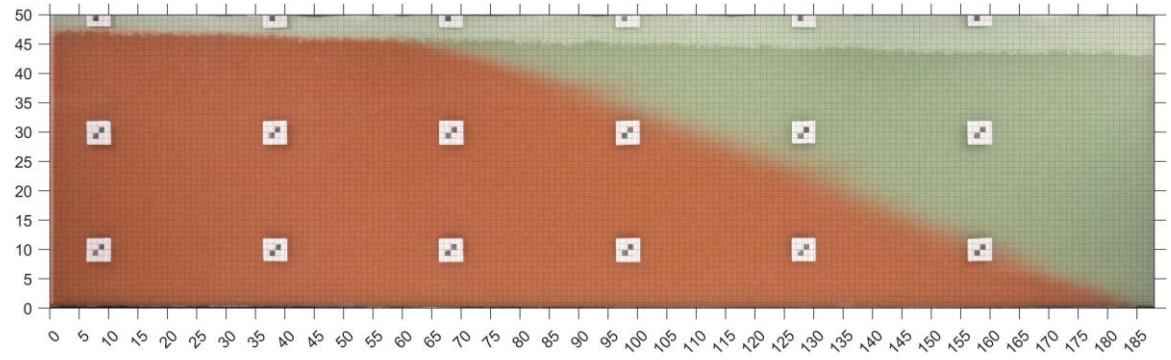

Figure 53 Sea water cline at t= 50 min for the active intrusion hSEA = 40 cm;hINLAND=36 cm

Impermeable barrier

Influence of the partially penetrated impermeable barrier to sea water cline features for different conditions have been analyzed and presented below. For this purpose, mitigated conditions of the active sea water cline have been demonstrated for different gradients in Figure 54 to Figure 65 and Figure 66 to Figure 73.

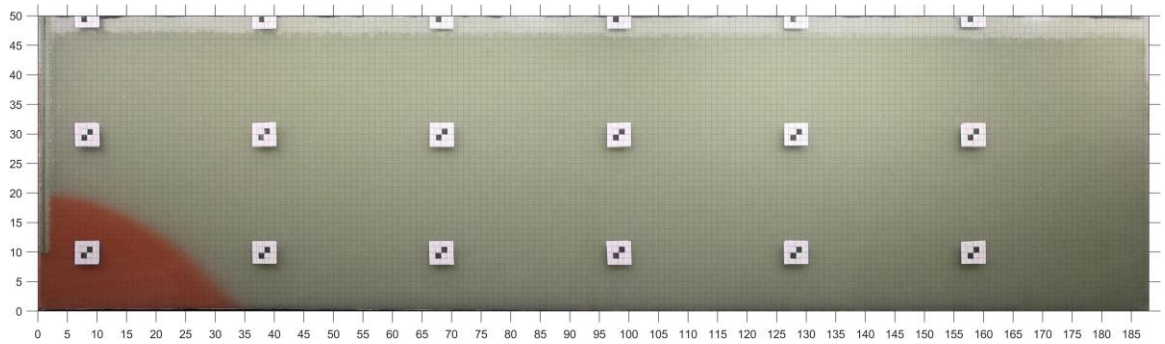

Figure 54 Sea water cline at t= 10 min for the active intrusion hSEA = 40 cm;hINLAND=39 cm and impermeable barrier depth d = 30 cm

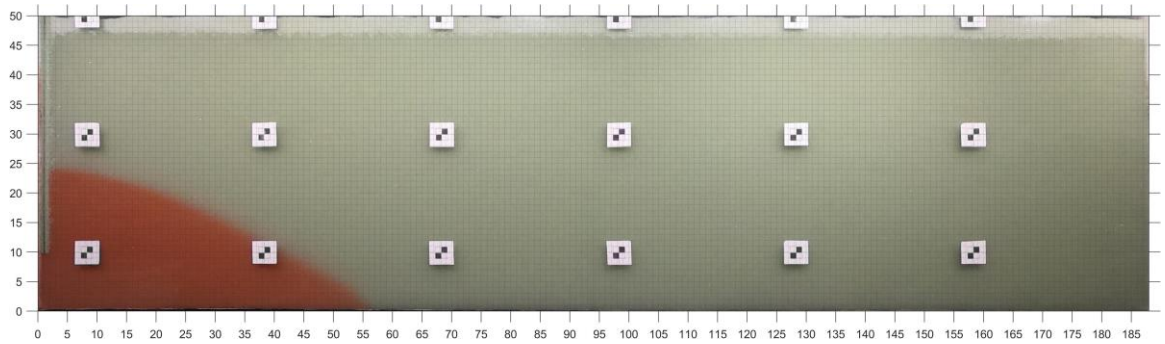

Figure 55 Sea water cline at t= 20 min for the active intrusion hSEA = 40 cm;hINLAND=39 cm and impermeable barrier depth d = 30 cm

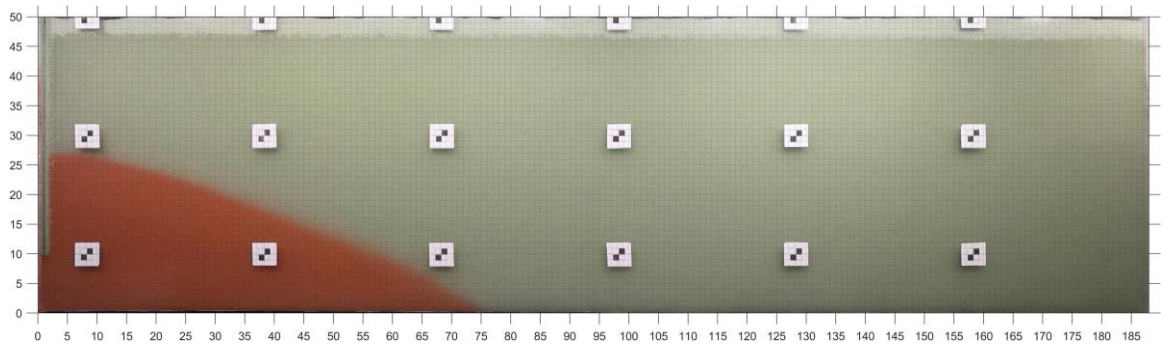

Figure 56 Sea water cline at t= 30 min for the active intrusion hSEA = 40 cm;hINLAND=39 cm and impermeable barrier depth d = 30 cm

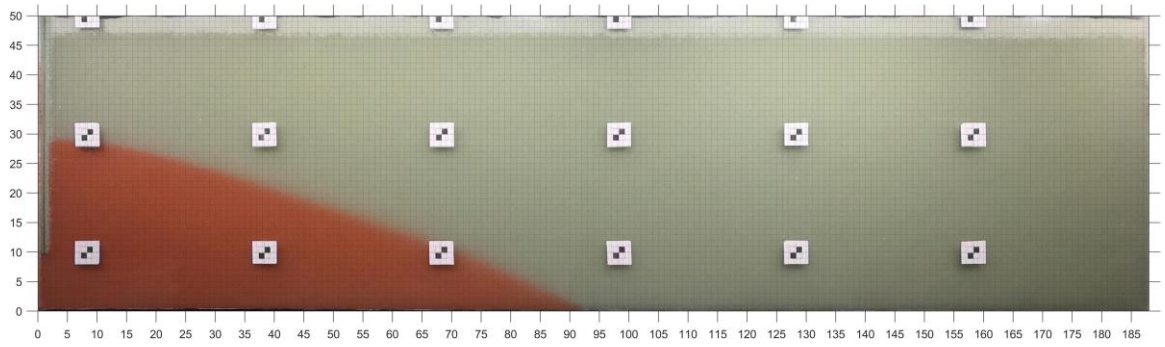

Figure 57 Sea water cline at t= 40 min for the active intrusion hSEA = 40 cm;hINLAND=39 cm and impermeable barrier depth d = 30 cm

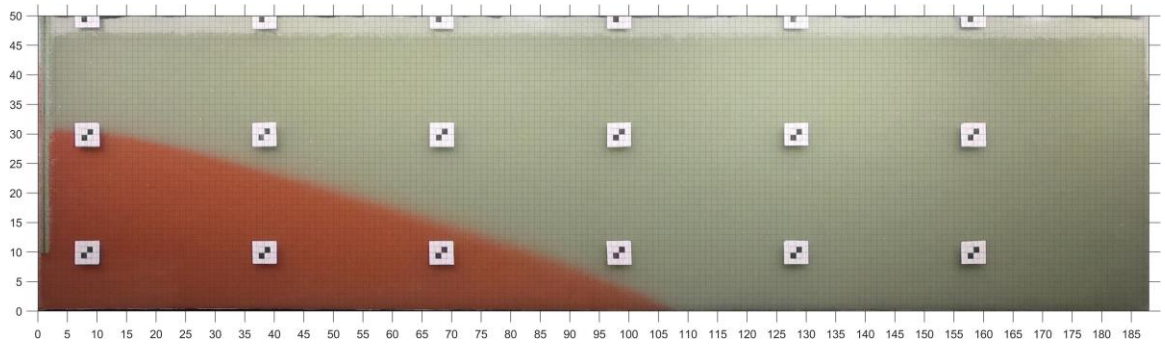

Figure 58 Sea water cline at t= 50 min for the active intrusion hSEA = 40 cm;hINLAND=39 cm and impermeable barrier depth d = 30 cm

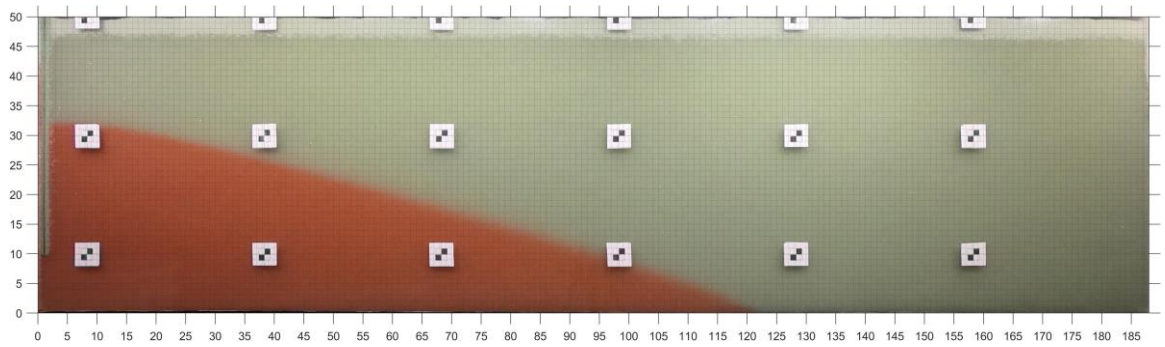

Figure 59 Sea water cline at t= 60 min for the active intrusion hSEA = 40 cm;hINLAND=39 cm and impermeable barrier depth d = 30 cm

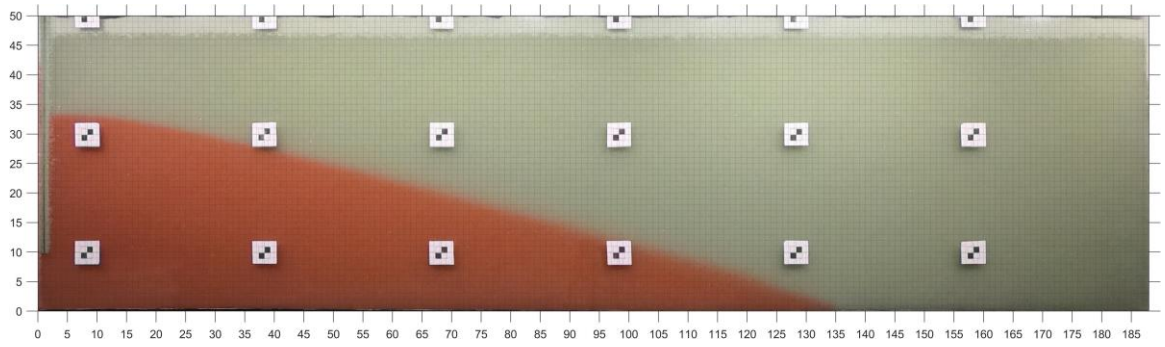

Figure 60 Sea water cline at t= 70 min for the active intrusion hSEA = 40 cm;hINLAND=39 cm and impermeable barrier depth d = 30 cm

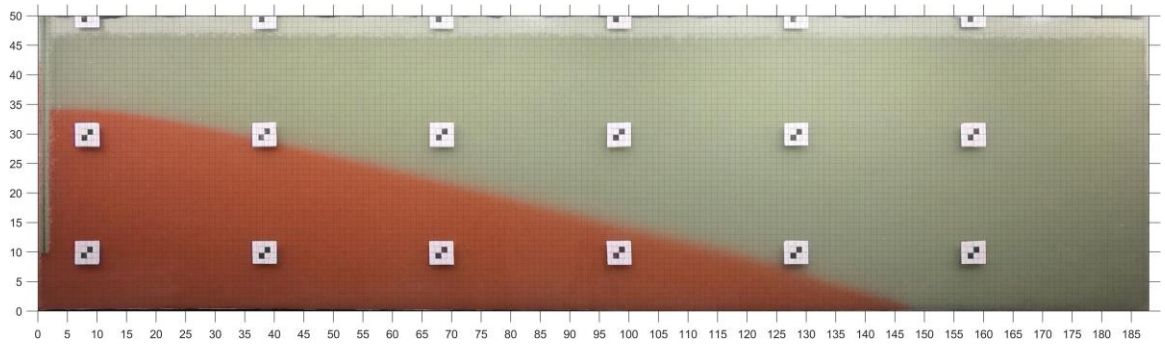

Figure 61 Sea water cline at t= 80 min for the active intrusion hSEA = 40 cm;hINLAND=39 cm and impermeable barrier depth d = 30 cm

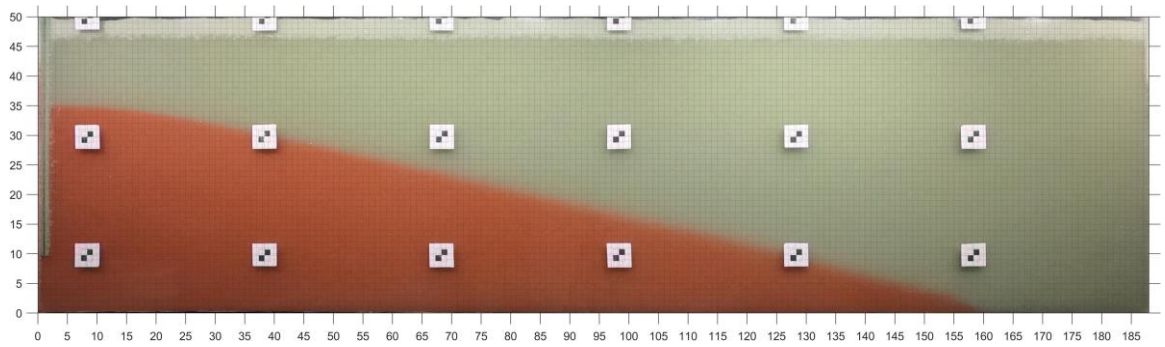

Figure 62 Sea water cline at t= 90 min for the active intrusion hSEA = 40 cm;hINLAND=39 cm and impermeable barrier depth d = 30 cm

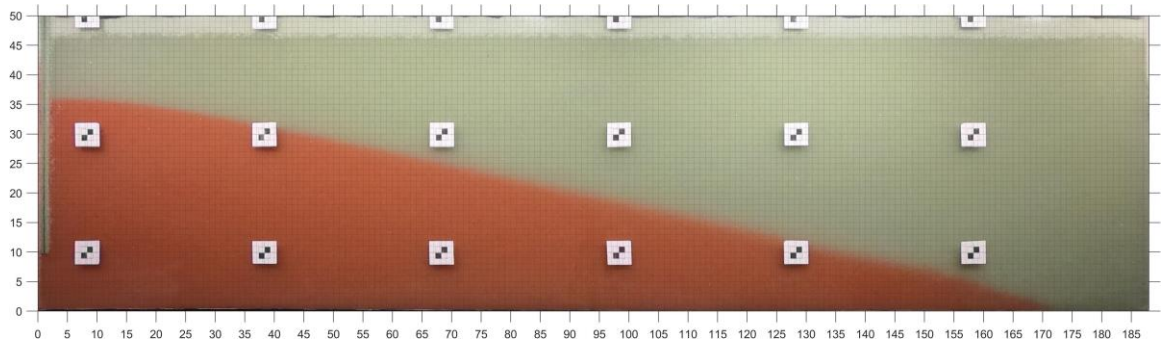

Figure 63 Sea water cline at t= 100 min for the active intrusion hSEA = 40 cm;hINLAND=39 cm and impermeable barrier depth d = 30 cm

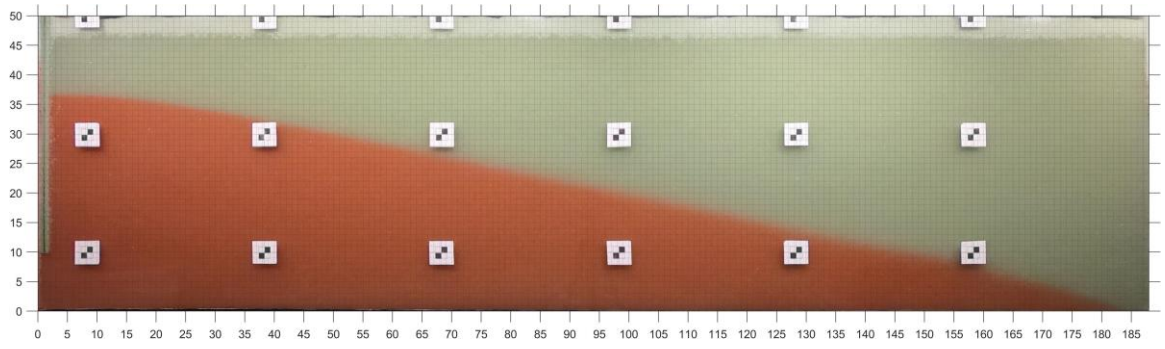

Figure 64 Sea water cline at t= 110 min for the active intrusion hSEA = 40 cm;hINLAND=39 cm and impermeable barrier depth d = 30 cm

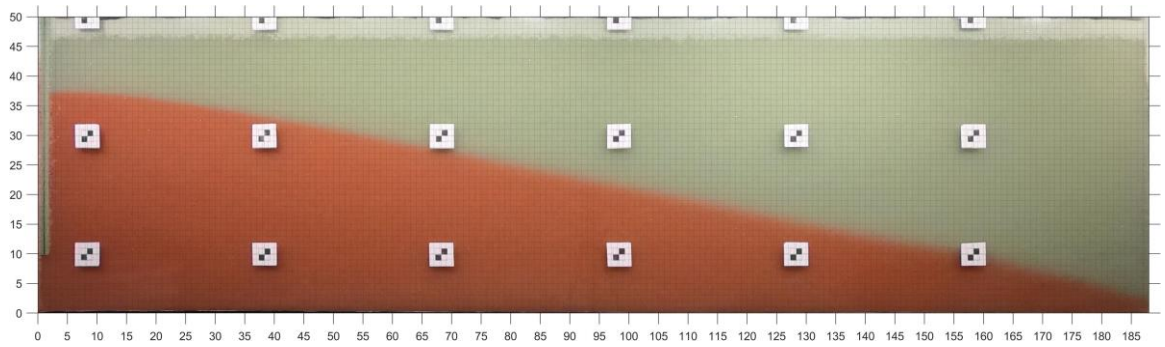

Figure 65 Sea water cline at t= 120 min for the active intrusion hSEA = 40 cm;hINLAND=39 cm and impermeable barrier depth d = 30 cm

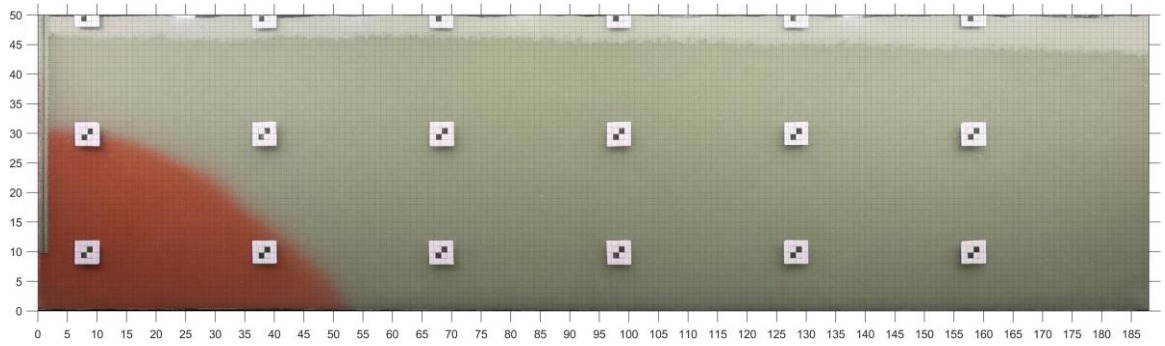

Figure 66 Sea water cline at t= 10 min for the active intrusion hSEA = 40 cm;hINLAND=36 cm and impermeable barrier depth d = 30 cm

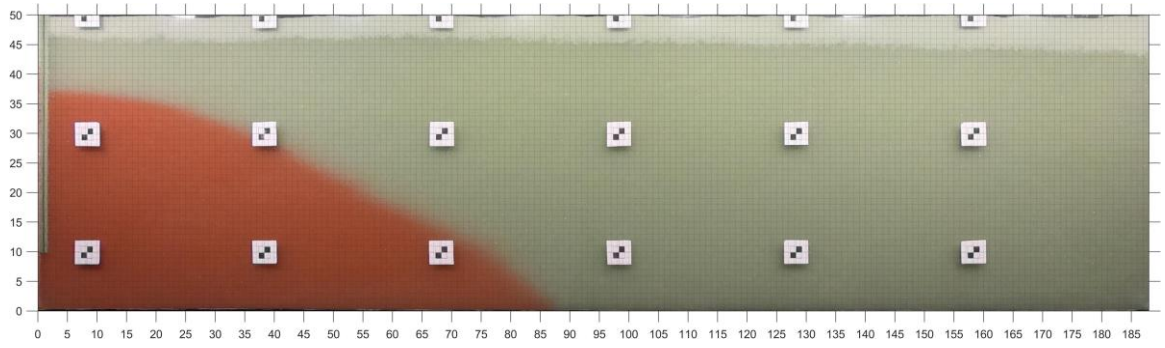

Figure 67 Sea water cline at t= 20 min for the active intrusion hSEA = 40 cm;hINLAND=36 cm and impermeable barrier depth d = 30 cm

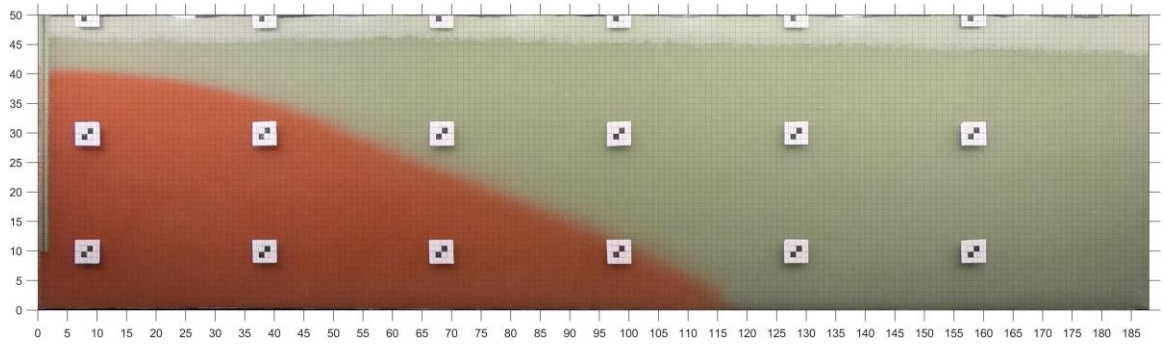

Figure 68 Sea water cline at t= 30 min for the active intrusion hSEA = 40 cm;hINLAND=36 cm and impermeable barrier depth d = 30 cm

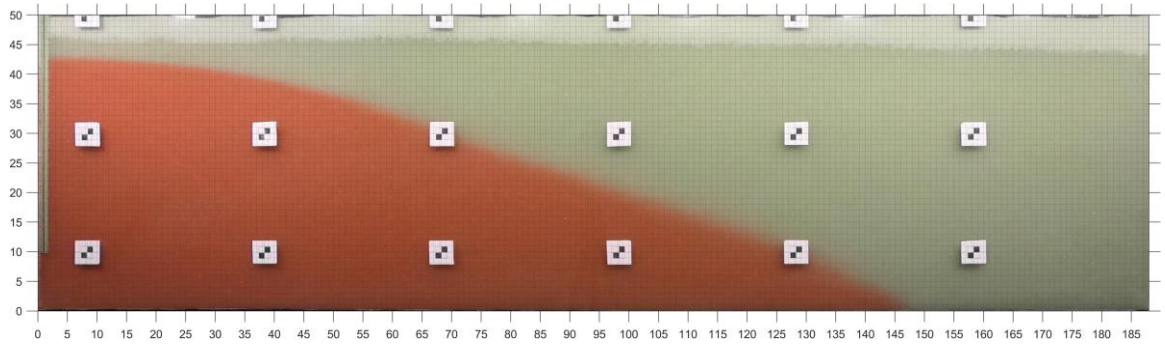

Figure 69 Sea water cline at t= 40 min for the active intrusion hSEA = 40 cm;hINLAND=36 cm and impermeable barrier depth d = 30 cm

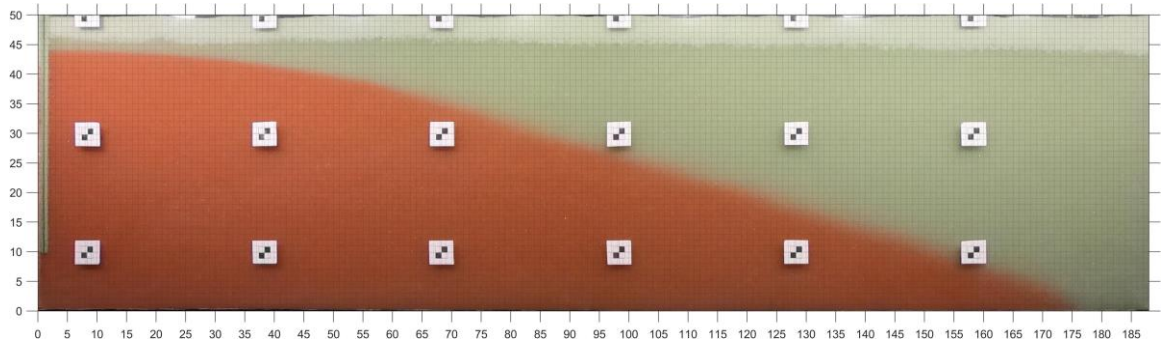

Figure 70 Sea water cline at t= 50 min for the active intrusion h_{SEA} = 40 cm;h_{INLAND}=36 cm and impermeable barrier depth d = 30 cm

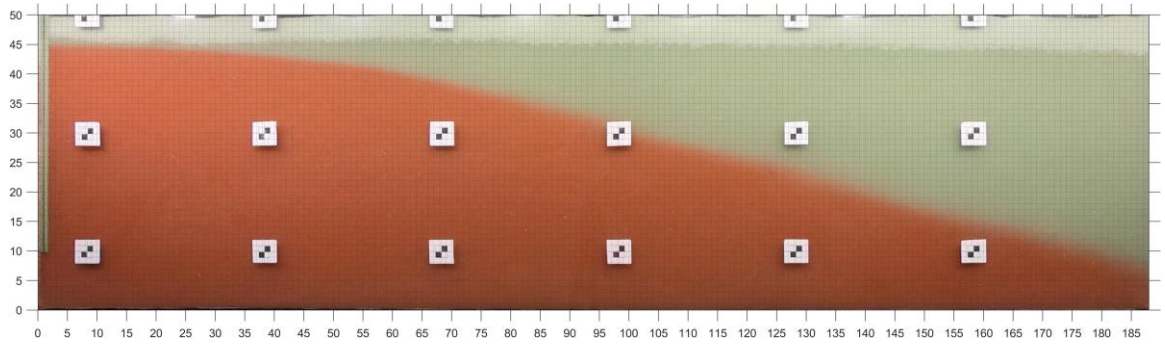

Figure 71 Sea water cline at t= 60 min for the active intrusion hSEA = 40 cm;hINLAND=36 cm and impermeable barrier depth d = 30 cm

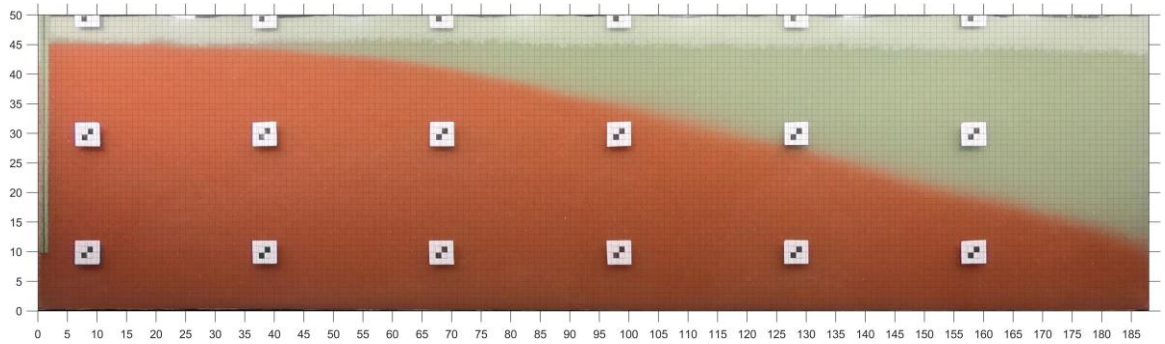

Figure 72 Sea water cline at t= 70 min for the active intrusion hSEA = 40 cm;hINLAND=36 cm and impermeable barrier depth d = 30 cm

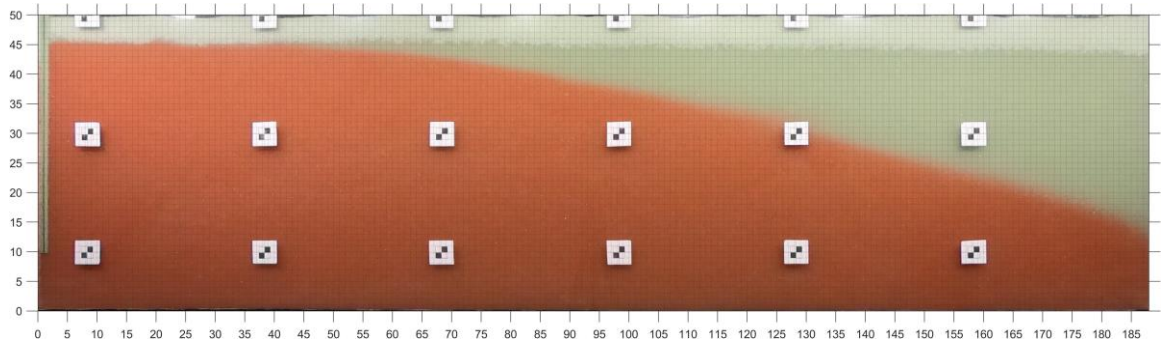

Figure 73 Sea water cline at t= 80 min for the active intrusion hSEA = 40 cm;hINLAND=36 cm and impermeable barrier depth d = 30 cm

Recharge channel

Influence of the partially penetrated impermeable barrier to sea water cline features for different conditions have been analyzed and presented below. For this purpose, mitigated conditions of the active sea water cline have been demonstrated for different gradients in Figure 74 to Figure 81 and Figure 82 to Figure 88.

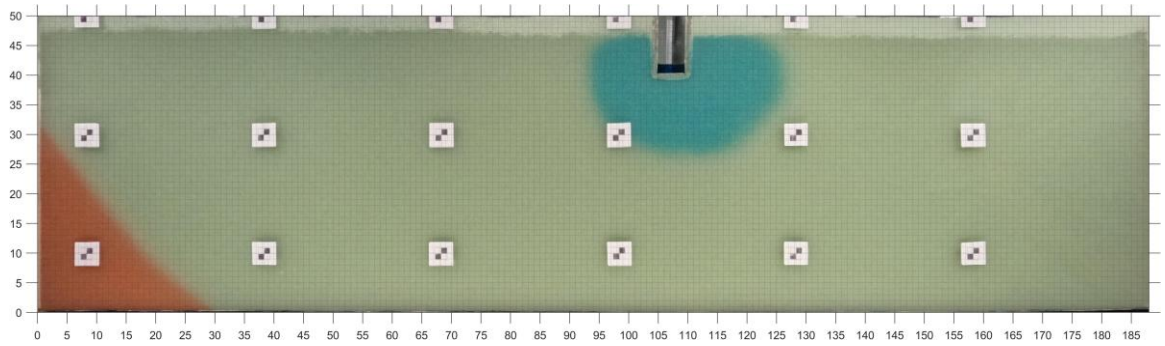

Figure 74 Sea water cline at t= 10 min for the active intrusion hSEA = 40 cm;hINLAND=39 cm and recharge channel with fresh water depth d = 1.75 cm

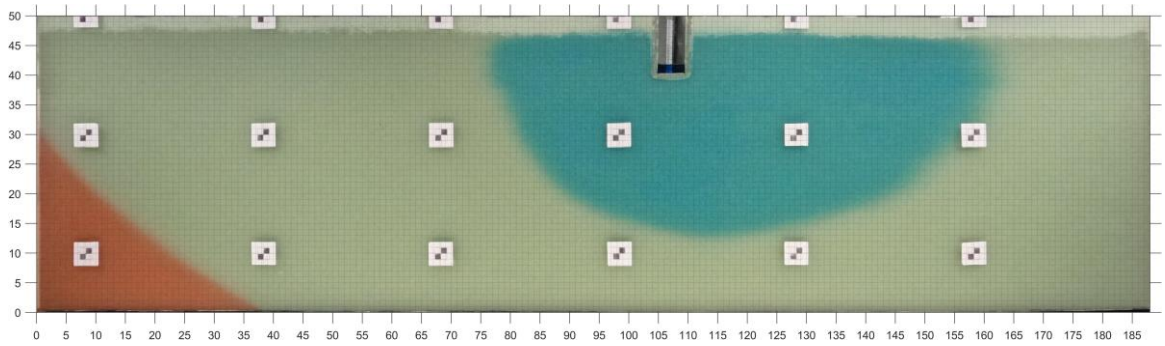

Figure 75 Sea water cline at t= 20 min for the active intrusion hSEA = 40 cm;hINLAND=39 cm and recharge channel with fresh water depth d = 1.75 cm

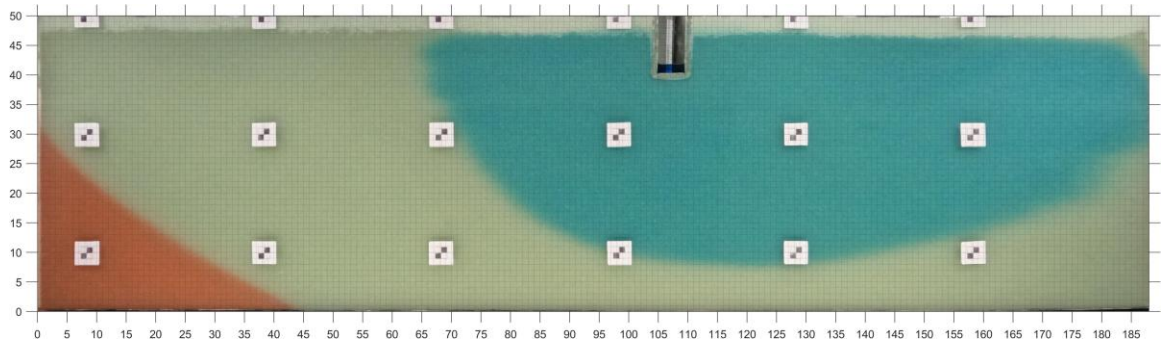

Figure 76 Sea water cline at t= 30 min for the active intrusion hSEA = 40 cm;hINLAND=39 cm and recharge channel with fresh water depth d = 1.75 cm

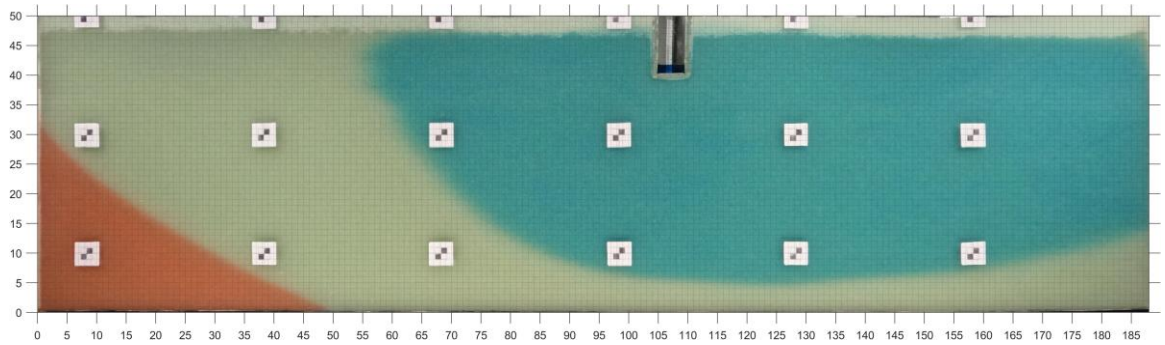

Figure 77 Sea water cline at t= 40 min for the active intrusion hSEA = 40 cm;hINLAND=39 cm and recharge channel with fresh water depth d = 1.75 cm

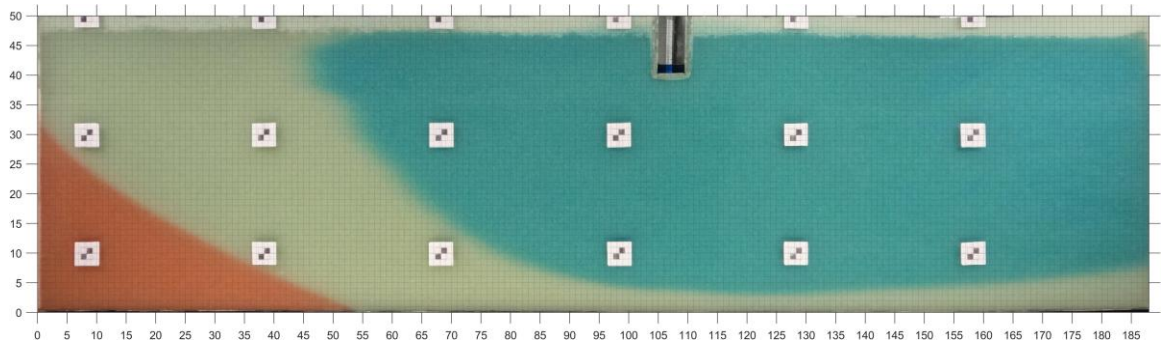

Figure 78 Sea water cline at t= 50 min for the active intrusion hSEA = 40 cm;hINLAND=39 cm and recharge channel with fresh water depth d = 1.75 cm

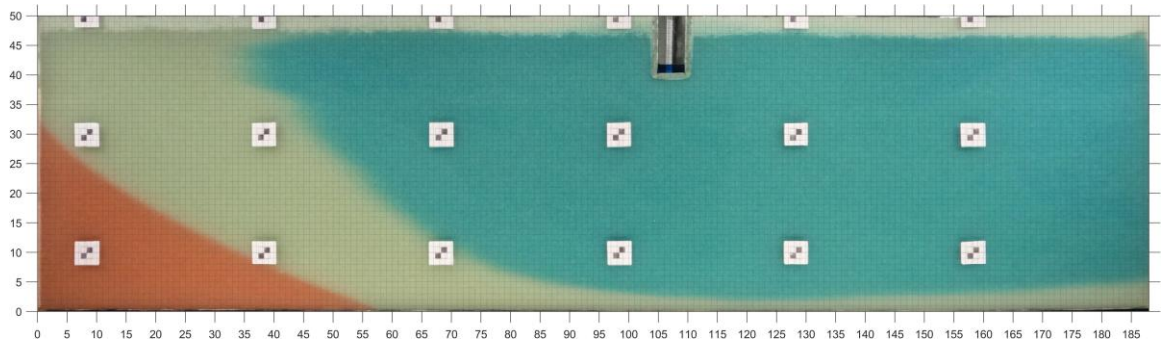

Figure 79 Sea water cline at t= 60 min for the active intrusion hSEA = 40 cm;hINLAND=39 cm and recharge channel with fresh water depth d = 1.75 cm

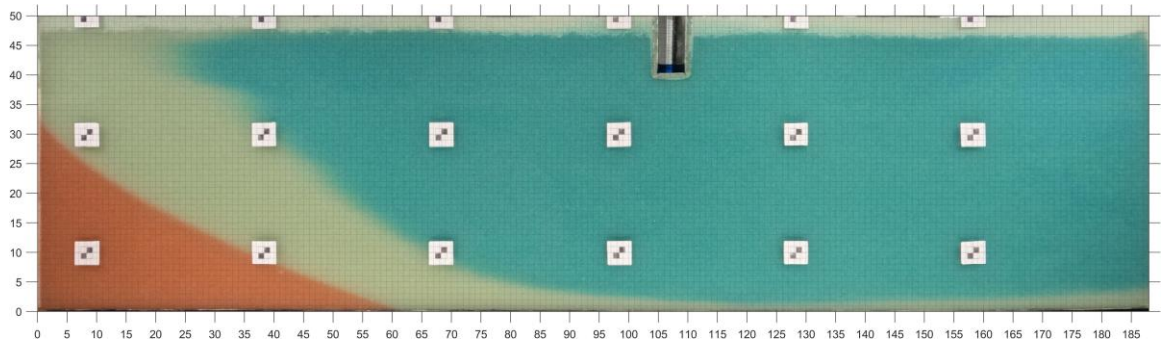

Figure 80 Sea water cline at t= 70 min for the active intrusion hSEA = 40 cm;hINLAND=39 cm and recharge channel with fresh water depth d = 1.75 cm

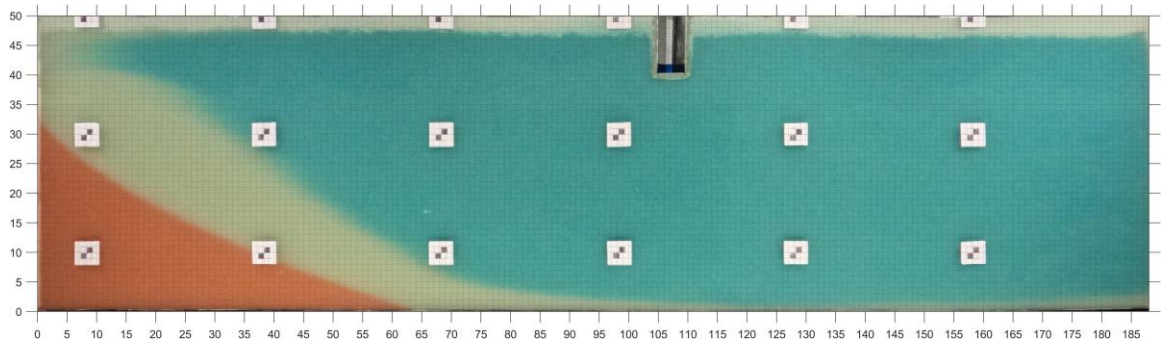

Figure 81 Sea water cline at t= 80 min for the active intrusion hSEA = 40 cm;hINLAND=39 cm and recharge channel with fresh water depth d = 1.75 cm

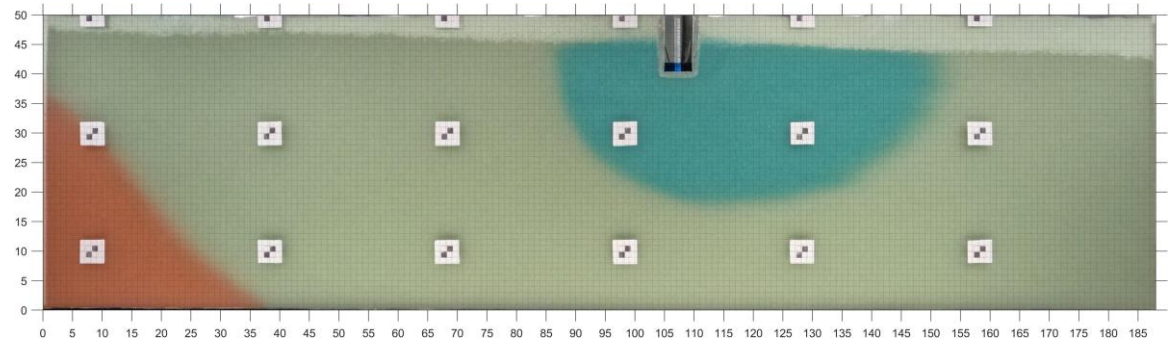

Figure 82 Sea water cline at t= 10 min for the active intrusion hSEA = 40 cm;hINLAND=36 cm and recharge channel with fresh water depth d = 1.75 cm

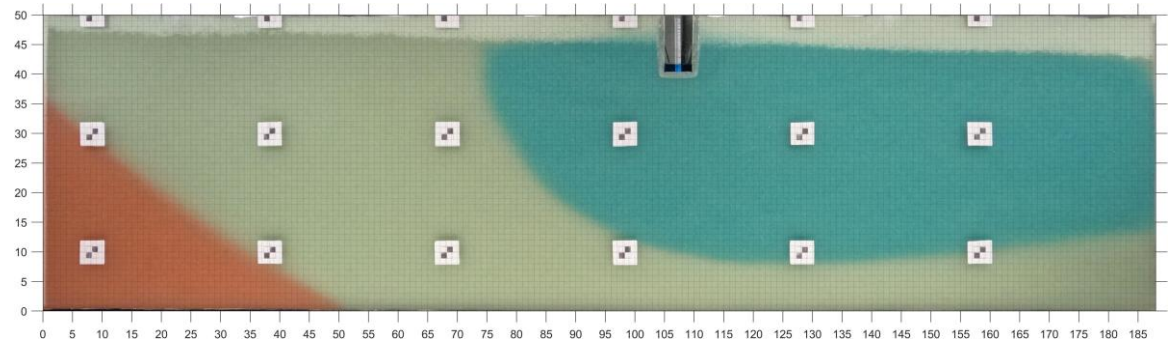

Figure 83 Sea water cline at t= 20 min for the active intrusion hSEA = 40 cm;hINLAND=36 cm and recharge channel with fresh water depth d = 1.75 cm

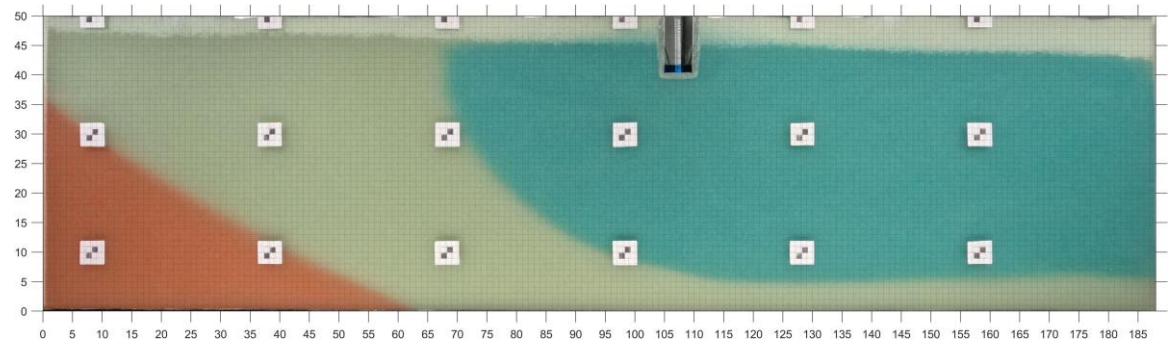

Figure 84 Sea water cline at t= 30 min for the active intrusion hSEA = 40 cm;hINLAND=36 cm and recharge channel with fresh water depth d = 1.75 cm

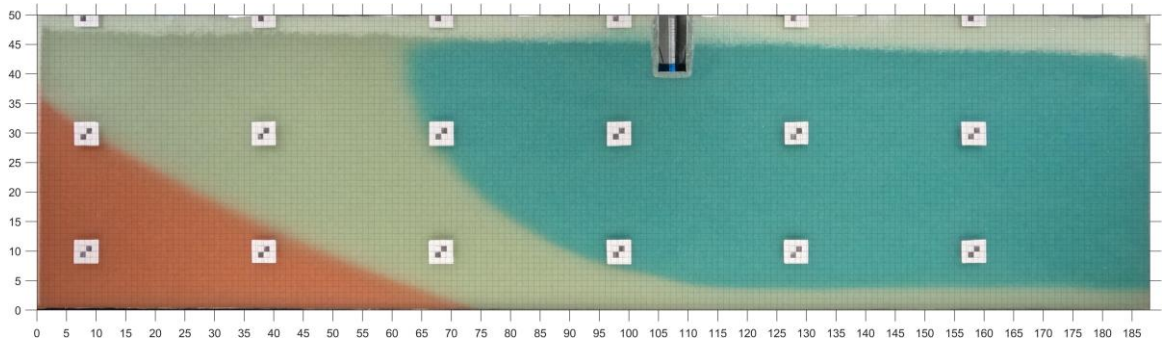

Figure 85 Sea water cline at t= 40 min for the active intrusion hSEA = 40 cm;hINLAND=36 cm and recharge channel with fresh water depth d = 1.75 cm

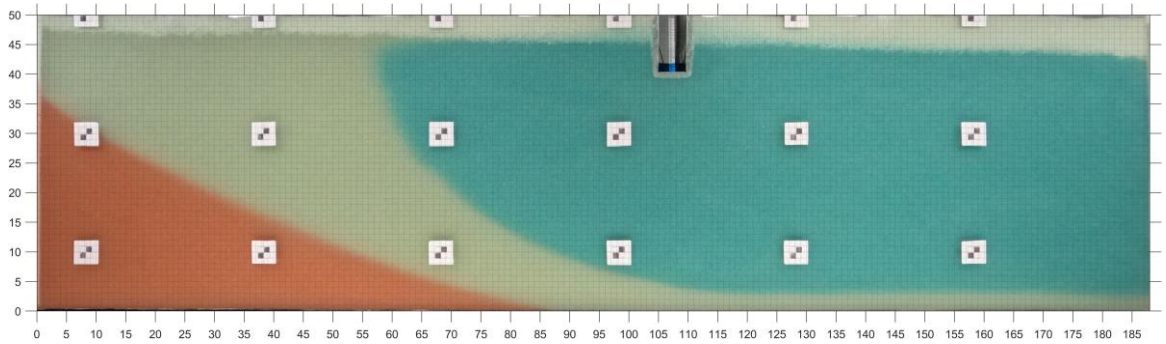

Figure 86 Sea water cline at t= 50 min for the active intrusion hSEA = 40 cm;hINLAND=36 cm and recharge channel with fresh water depth d = 1.75 cm

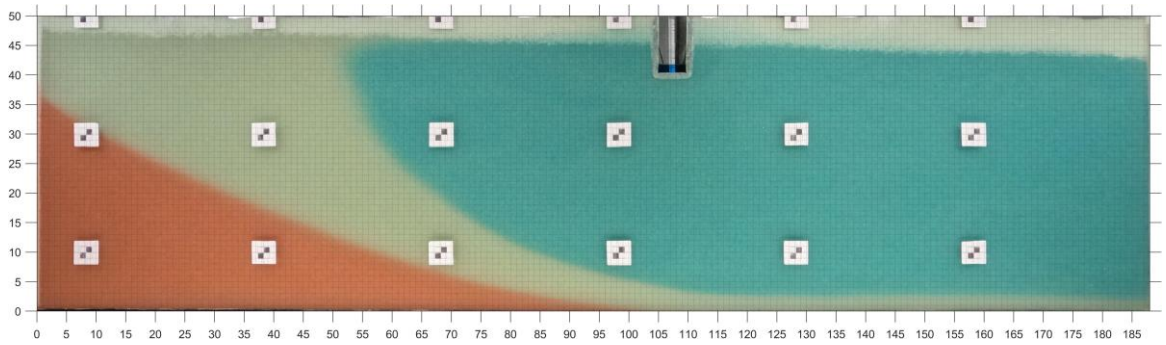

Figure 87 Sea water cline at t= 60 min for the active intrusion hSEA = 40 cm;hINLAND=36 cm and recharge channel with fresh water depth d = 1.75 cm

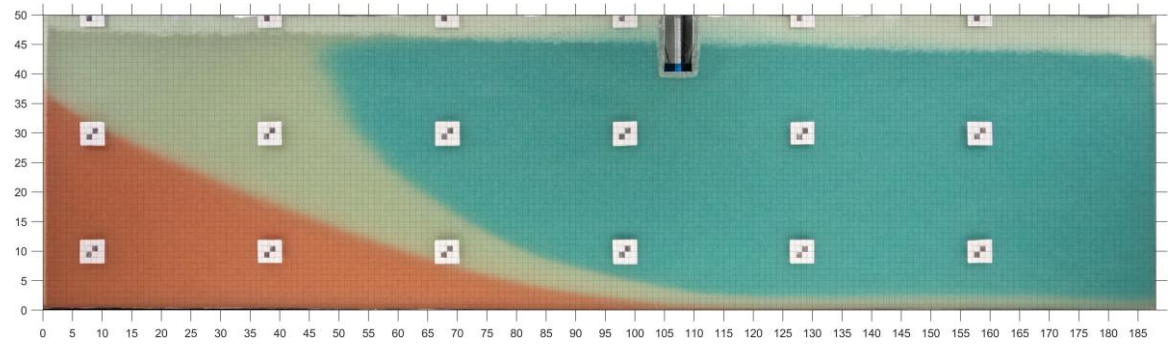

Figure 88 Sea water cline at t= 70 min for the active intrusion hSEA = 40 cm;hINLAND=36 cm and recharge channel with fresh water depth d = 1.75 cm

Criteria for the assessment of tested mitigation measures - positive and negative effects of active intrusion

Definition

The effectiveness of tested mitigation measures has been determined via several criteria which were recognized and selected as highly impacting the salinity regime within the project area. Primary focus is set up to sea water cline geometry and spatio-temporal features. In this way it is easy to distinguish whether the sea water affects the aquifer surface area representing the pedological layer suitable for the root development.

Two main criteria contributing to the determination of the mitigation measures effectiveness are as follows:

- Sea water cline to length;
- Sea water cline wedge height.

Identification and assessment

Both aforementioned criteria have been tested and presented below. Figure 89 and Figure 90 demonstrate the sensitivity of the sea water cline shape and size to gradients between the sea water source and inland water table. Implementation and effectiveness of the impermeable barrier to mitigate sea water intrusion have been demonstrated in Figure 91 and Figure 92while the prevention of the sea water intrusion caused by the recharge channel is demonstrated in Figure 93 and Figure 94.

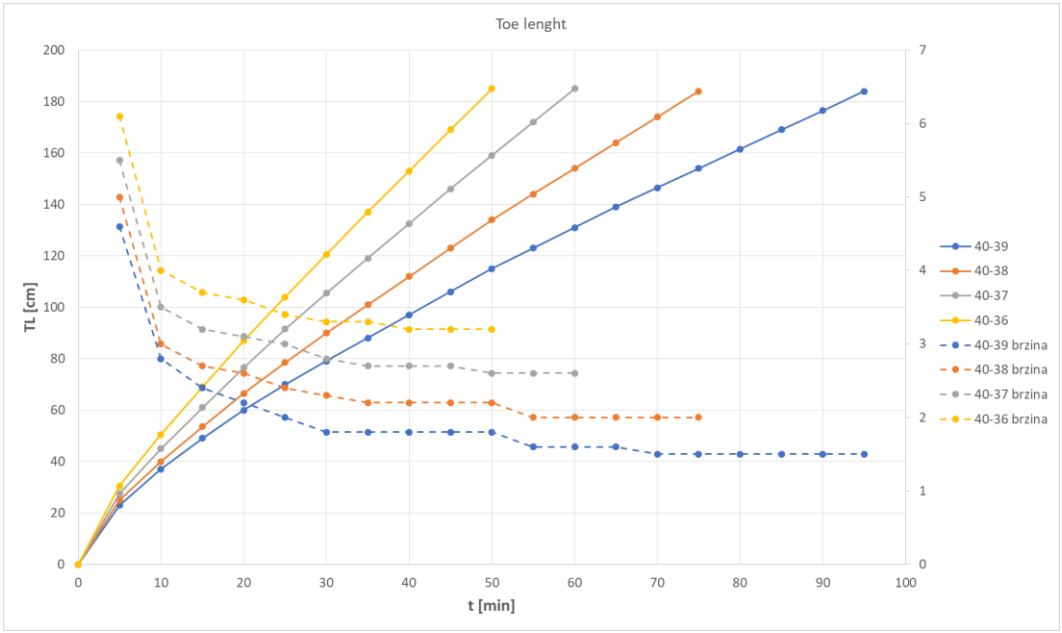

Figure 89Sea water cline toe length and intrusion velocity for the active intrusion and variable gradients

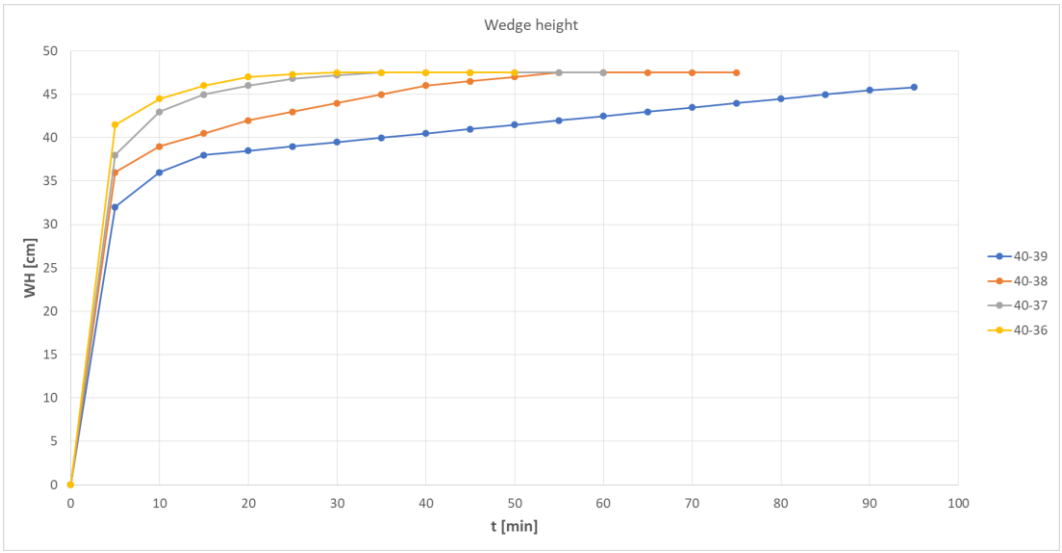

Figure 90 Sea water cline wedge height for the active intrusion and variable gradients

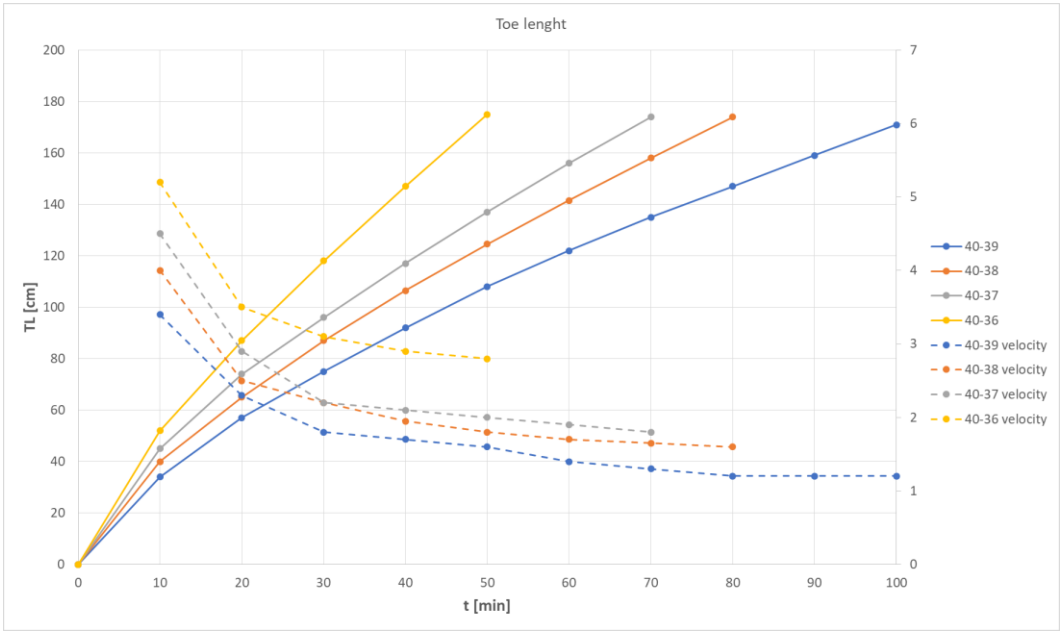

Figure 91 Sea water cline toe length and intrusion velocity for the active intrusion variable gradients and impermeable barrier depth d = 30 cm

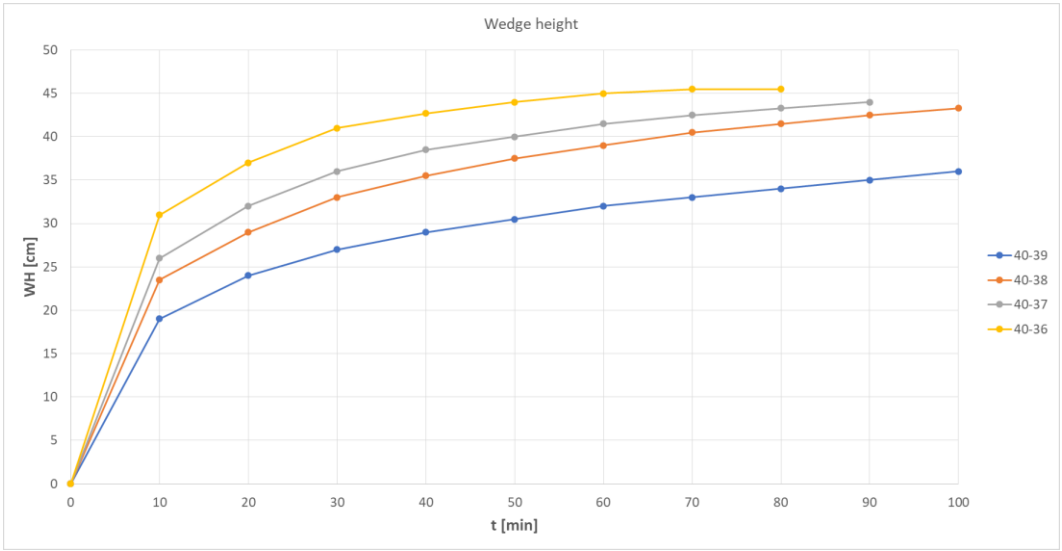

Figure 92 Sea water cline wedge height for the active intrusion variable gradients and impermeable barrier depth d = 30 cm

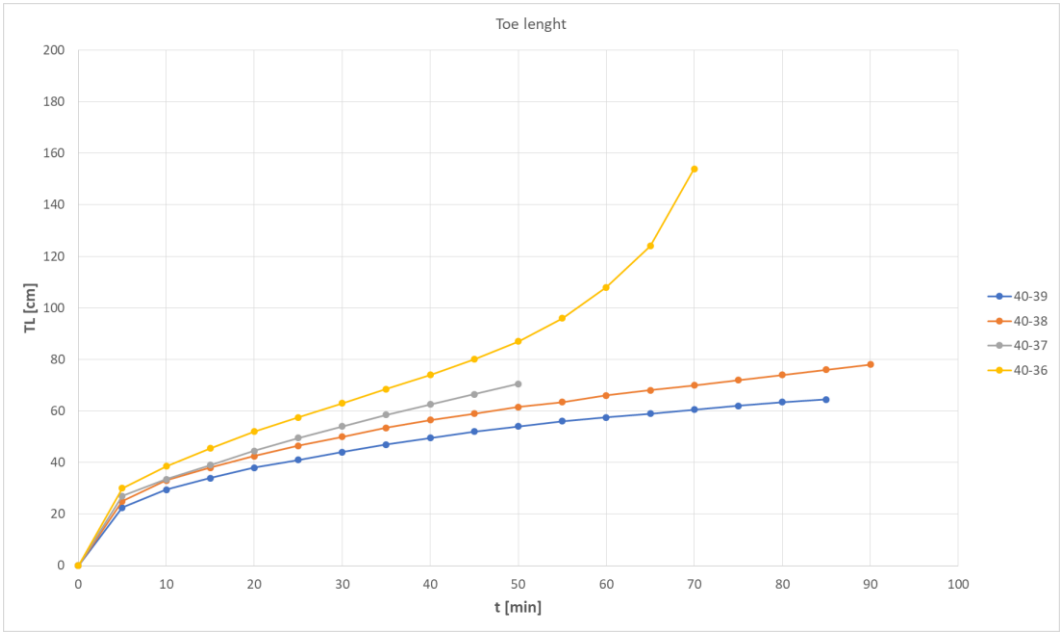

Figure 93 Sea water cline toe length for the active intrusion variable gradients and recharge channel water depth d = 1.75 cm

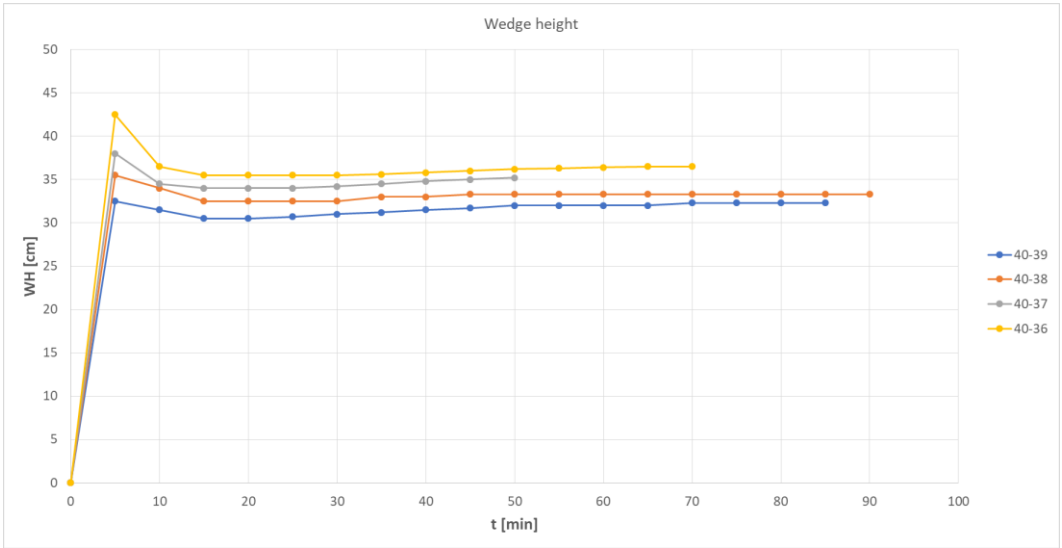

Figure 94 Sea water cline wedge height for the active intrusion variable gradients and recharge channel water depth d = 1.75 cm

Positive and negative facts about tested mitigation measures

Impermeable barrier

Positive facts

- Easy to implement due the limited penetration depth. Since the primary goal is to increase the quality of surface and ground water of the shallow unconfined aquifer, impermeable barrier should be performed to enter the clay aquitard layer. Following the outcomes of the geophysical in situ investigation work, expected penetration depth equals up to 12 m beneath the ground level.

Negative facts

- Due to the active sea water intrusion occurrence, partially or fully submerged impermeable barrier could not ensure the enhancement of the water quality but only decrease the sea water in flux to the inland. To ensure better water quality standard this mitigation measure should be accompanied with other appropriate mitigation techniques like irrigation system and/or groundwater extraction from the wells.

Recharge channel

Positive facts

- Infrastructure already exist. One of the melioration channels can be modified to recharge channel fed with water directly from the river Neretva, upwards from the water gates.
- Offers “constant in use” solution which does not require any mechanical either electrical supply.
- Highly effective and offers long term solution.

Negative facts

- Requires the intake building infrastructure at the left hand side of the river Neretva bed.

List of figures